iScience

CellPress
OPEN ACCESS

Article

Delta-Frequency Augmentation and Synchronization in Seizure Discharges and Telencephalic Transmission

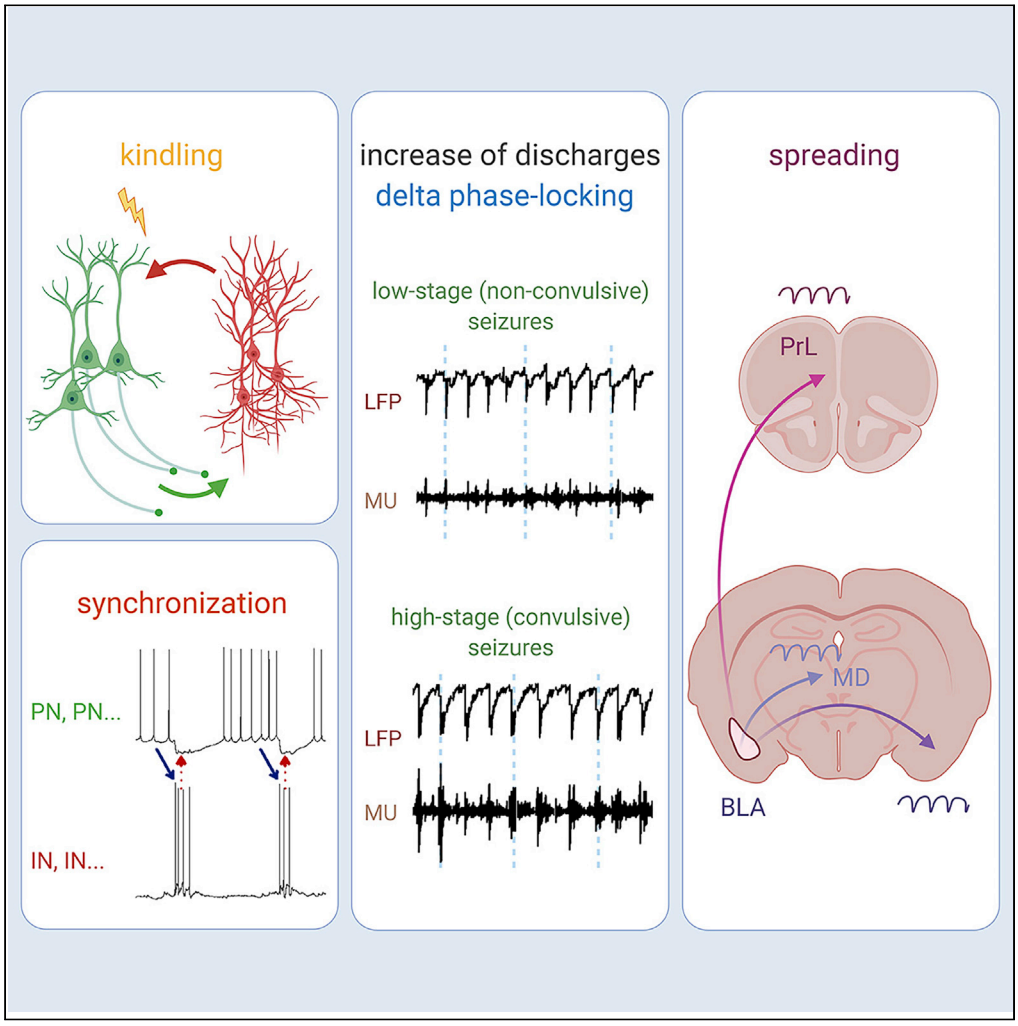

Ping Chou, Guan-Hsun Wang, Shu-Wei Hsueh, Ya-Chin Yang, Chung-Chin Kuo

ycyang@mail.cgu.edu.tw (Y.-C.Y.)
chungchinkuo@ntu.edu.tw (C.-C.K.)

HIGHLIGHTS

Delta oscillations constitute the natural frequencies in basolateral amygdala

Neuronal burst and interburst intervals set the wavelength for delta oscillations

Delta oscillations may be readily transmitted distantly and translated behaviorally

Synchrony precedes and outlasts increase in discharges and seizures in ictogenesis

Chou et al., iScience *23*, 101666
November 20, 2020 © 2020 The Authors.
https://doi.org/10.1016/j.isci.2020.101666

iScience

CellPress
OPEN ACCESS

Article

Delta-Frequency Augmentation and Synchronization in Seizure Discharges and Telencephalic Transmission

Ping Chou,[1,9] Guan-Hsun Wang,[2,3,4,8,9] Shu-Wei Hsueh,[5] Ya-Chin Yang,[2,5,6,10,*] and Chung-Chin Kuo[1,7,*]

SUMMARY

Epileptic seizures constitute a common neurological disease primarily diagnosed by characteristic rhythms or waves in the local field potentials (LFPs) of cerebral cortices or electroencephalograms. With a basolateral amygdala (BLA) kindling model, we found that the dominant frequency of BLA oscillations is in the delta range (1–5 Hz) in both normal and seizure conditions. Multi-unit discharges are increased with higher seizure staging but remain phase-locked to the delta waves in LFPs. Also, the change in synchrony precedes and outlasts the changes in discharging units as well as behavioral seizures. One short train of stimuli readily drives the pyramidal-inhibitory neuronal networks in BLA slices into prolonged reverberating activities, where the burst and interburst intervals may concurrently set a "natural wavelength" for delta frequencies. Seizures thus could be viewed as erroneous temporospatial continuums to normal oscillations in a system with a built-in synchronizing and resonating nature for information relay.

INTRODUCTION

Epileptic seizure discharges are paroxysmal, excessive, and synchronous activities, mostly from the amygdala, allocortices, and neocortices in the forebrain, where a salient input must be promptly coded and appropriately responded to (French et al., 1956; McCormick and Contreras, 2001; Penfield and Jasper, 1954). Self-repetitive oscillating rhythmic or semi-rhythmic waves in electroencephalograms from patients or local field recordings from experimental animals constitute the pathognomonic features of the disease. An increase in the power of the theta/delta bands or in the theta/alpha ratio during seizures has been reported in experimental animals or patients (Ali et al. 2013; Faught et al., 1992; Goddard et al., 1969; Pinault et al., 2001; Monto et al., 2007; Motaghi et al., 2012; Jalilifar et al., 2016). On the other hand, Musto et al. (2009) showed that frequencies above 20 Hz were more prevalent in high-stage seizures. Tsuchiya and Kogure (2011) maintained that successful kindling with stimulation of the right hippocampus enhances relative power of the high (12–30 Hz) than the low (0–9 Hz) frequency band. There are thus apparent controversies on the predominant frequencies in epileptic seizures. This may be partly ascribed to methodological differences, including experimental models, designated windows of staging, or timings after the trigger of seizures. But it also underscores the imperativeness of more mechanistic investigations into the basic attributes underlying the phenomenal oscillations in local field potentials (LFPs).

Brain waves, or time-dependent deflection of LFPs, are in essence integrated changes in local currents contributed by cellular activities. Epileptic seizures are characteristically composed of burst discharges (Siniscalchi et al., 1997; Yaari and Beck, 2002), which implicate strong cellular activities clustered in a short time, and thus conceivably a manifest effect on LFPs. In the network level, a temporospatially adequate involvement of the telencephalic oscillation systems presumably is responsible for the behavioral manifestations of seizures (Hamer et al., 1999, 2003). Because neuronal burst discharges and network oscillations also exist in normal conditions (Connors and Gutnick, 1990; Jefferys et al., 2012; Schnitzler and Gross, 2005), it is very much desirable to differentiate physiological and pathophysiological (e.g., seizure) discharges and consequent network oscillations. Burst discharges may act as an autonomous or segregating code interrupting information flow, but they may also be transmitted or act as a modulating code modifying the pace and pathway of information flow with concomitant synaptic plasticity (Lisman, 1997; Remy and Spruston, 2007; Thomas et al., 1998). It is thus desirable to decipher how the cellular burst discharges are evolved and organized into abnormal network oscillations and consequently the augmented power in specific

[1]Department of Physiology, National Taiwan University College of Medicine, 1 Jen-Ai Road, 1st Section, Taipei 100, Taiwan

[2]Department of Biomedical Sciences, College of Medicine, Chang Gung University, 259 Wen-Hwa 1st Road, Kwei-Shan, Tao-Yuan 333, Taiwan

[3]School of Medicine, College of Medicine, Chang Gung University, Tao-Yuan, Taiwan

[4]Department of Medical Education, Chang Gung Memorial Hospital, Linkou Medical Center, Tao-Yuan, Taiwan

[5]Graduate Institute of Biomedical Sciences, College of Medicine, Chang Gung University, Tao-Yuan, Taiwan

[6]Neuroscience Research Center, Chang Gung Memorial Hospital, Linkou Medical Center, Tao-Yuan, Taiwan

[7]Department of Neurology, National Taiwan University Hospital, Taipei, Taiwan

[8]Present address: Department of Neurology, Chang Gung Memorial Hospital, Linkou Medical Center, Tao-Yuan, Taiwan.

[9]These authors contributed equally

[10]Lead contact

*Correspondence: ycyang@mail.cgu.edu.tw (Y.-C.Y.), chungchinkuo@ntu.edu.tw (C.-C.K.)

https://doi.org/10.1016/j.isci.2020.101666

This is an open access article under the CC BY-NC-ND license (http://creativecommons.org/licenses/by-nc-nd/4.0/).

frequency bands in seizures. Also, if the seemingly chaotic multi-unit neuronal discharges could be organized into more regular network oscillations embodied in the increased power in spectral analysis, could the predominant oscillations in the epileptogenic focus be faithfully transmitted to the other brain structures and translated into seizure behaviors? In this regard, how would the abnormal synchronization and excessiveness of cellular activities, the two fundamental attributes of epileptic seizures, be orchestrated to make the characteristic LFP and behavioral oscillations during ictogenesis?

The amygdaloid complex could be simplistically divided into two major parts, the cortex-like basolateral and striatum-like central nuclei (BLA and CEA) with smaller aggregates of GABAergic neurons (the intercalated nuclei) in between (Paré et al., 2003). The BLA contains glutamatergic projection neurons (PNs) as well as a smaller number of GABAergic interneurons (INs) (Capogna, 2014; Muller et al., 2006). The spontaneous firing rates of PN are typically low (<1 Hz), presumably ascribable to the abundant IN inputs to the soma and proximal processes of PN (McDonald and Betette, 2001). Consistently, the membrane potential of PNs is dominated by the inhibitory postsynaptic potentials (IPSPs) contributed by INs, which have stronger baseline activities (Lang and Paré, 1998; Paré et al., 2003; Spampanato et al., 2011). In addition to the intimacy of PN-IN wirings, BLA is well known for its susceptibility to kindling, which vividly demonstrates how a normal circuitry could be rapidly turned epileptic with just changes in activities (McIntyre and Gilby, 2008). BLA therefore is an ideal system for the exploration of the biophysical rationales of physiological and pathophysiological PN-IN oscillations and thus the basic mechanisms underlying the cellular basis of the phenomenal LFP oscillations and normal-ictal transitions. Also, the transmission of the unilateral BLA epileptiform multi-unit discharges and LFP changes to the other structures could be temporospatially characterized to elucidate the progress of network oscillations as well as the relative roles of increased discharges/enhanced synchrony underlying the electrophysiological and behavioral ictogenesis. With combined *in vivo* and *in vitro* electrophysiological recordings and behavioral observations, we found that amygdala kindling and epileptogenesis are based on increased burst discharges in PNs and especially INs. The duration of the reverberating burst discharges set a "natural wavelength" and thus frequency of network oscillation, which is in the delta band in either normal or seizure conditions. The delta oscillations could then be readily transmitted to the other distant brain structures and cause corresponding behavioral manifestations, like resonance at common natural frequencies. Moreover, enhanced synchrony seems to be an even more fundamental attribute of ictogenesis and comes before as well as goes after the increase in discharges.

RESULTS

Amygdala Kindling Induces Afterdischarges with an Oscillating Frequency at ~1–5 Hz

Figure 1A shows the afterdischarges (ADs) following just the first session of a standard kindling stimuli applied to the left BLA. If compared with the baseline recordings, the ADs are characterized by a marked increase in rhythmic waves in LFP. It is interesting that ADs may develop not only in the left but very often (>80%) also in the right BLA and could manifest in a wax-and-wane pattern with variable kinetics (Figure 1A). It is evident that the LFP shows the highest relative power at a frequency of ~1–5 Hz (on average ~3 Hz), which the baseline discharges also mimic, although the absolute peak is much smaller (Figure 1B). Moreover, the coherence between the LFP in the right and left BLA is also the highest at ~1–5 Hz (Figure 1C). Also, the peak power at the delta band always remains very similar for the ADs following a very wide frequency range of the kindling stimuli between 5 and 500 Hz (Figures 1D–1F), as if the BLA circuitry has a well preserved "natural frequency" of oscillation. Seizure discharges following kindling are thus characterized by a marked increase in power, but an unchanged basic frequency, of network oscillations involving bilateral BLA.

The Number of Discharge Units and Delta Power Both Increase with Escalating Behavioral Seizures

We endeavored to relate the cellular origin and behavioral consequences of the markedly increased network delta power. The behavioral manifestations of seizures usually get more severe with more sessions of kindling stimulation. We simplistically classified behavioral seizures into a low stage (all kinds of behavioral changes without any convulsions, roughly Racine stages 0.5–2) and a high stage (the presence of focal or generalized convulsions, signaling stronger oscillations in the motor cortex and relevant circuitry for motor execution, roughly Racine stages 3–5) for a very basic and clear-cut differentiation. The ADs following kindling stimulation apparently oscillating in the delta band in LFP recordings could be further characterized by multi-unit (MU) discharges, which show a clear tendency to be grouped into "bursts" with the same

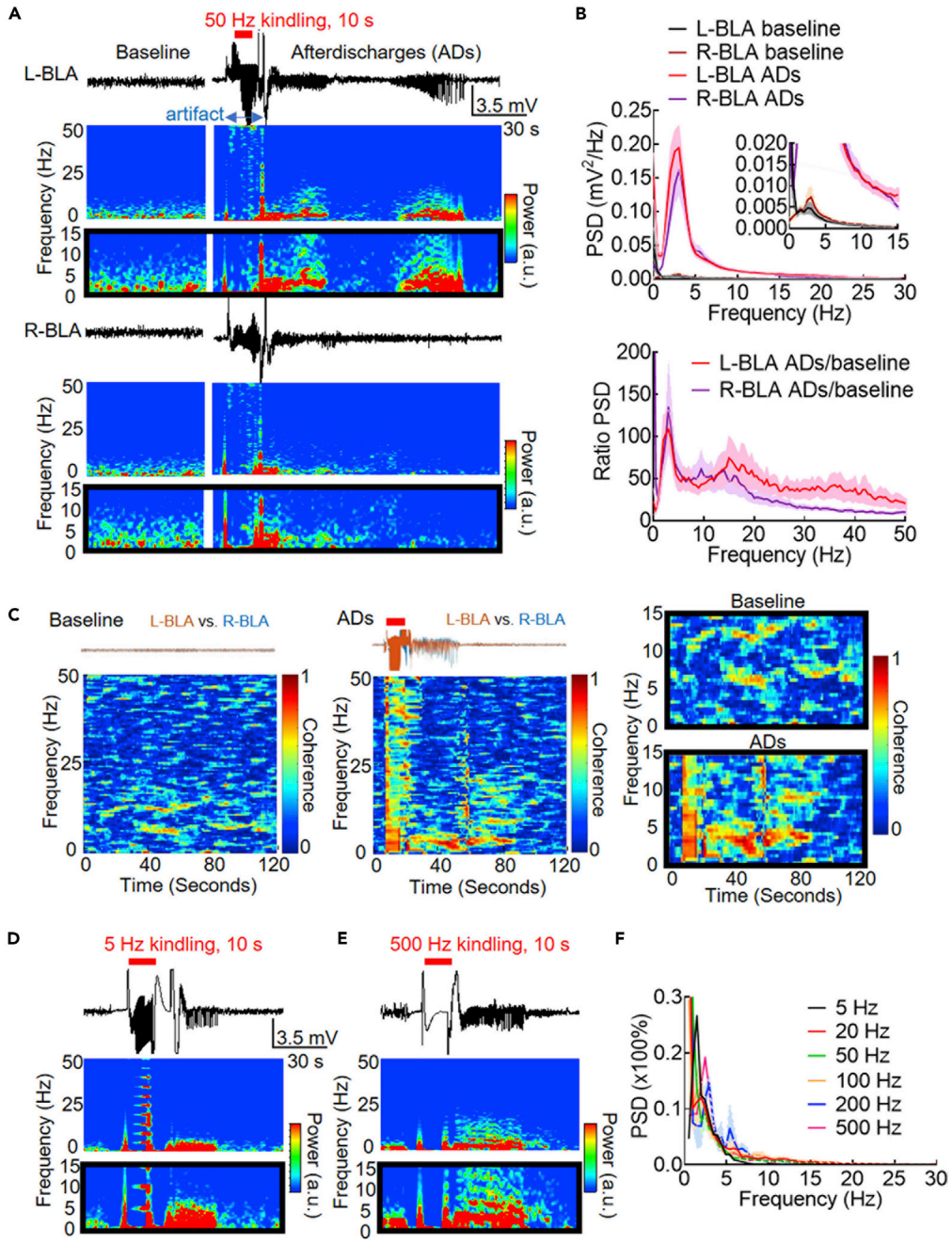

Figure 1. Electrical Stimulation of the Basolateral Amygdala (BLA) Induces Afterdischarges (ADs) in the Same Delta-Range Frequency as the Discharges at Baseline

(A) Sample local field potential (LFP, band pass filtering at 0.1–100 Hz, upper panel) recordings are obtained from the left and right basolateral amygdala (L- and R-BLA) 1 min before (baseline) and immediately after the second stimulation session of kindling applied only to the left BLA on the first day of a standard kindling procedure (biphasic pulse at ±170 μA, 1 ms each phase, 50 Hz × 10 s). Behaviorally the animal is in Racine stage 1. The artifact right before and after the 50 Hz stimulation was caused by connection and disconnection with the stimulus generator. In the concomitant time-frequency analysis (spectrograms, lower panel), the major power of the LFP during ADs is focused in the delta band (enlarged in black frames). The artifact before and after the 10-s stimulation session is due to engagement and disengagement of the stimulator.

(B) The power spectrum density (PSD, top) has a clear peak in the delta-range frequency for both baseline and ADs at both left and right BLA, although the power is much lower at baseline than in ADs (refer to the enlarged inset figures). The ratio

Figure 1. *Continued*
of PSD during ADs and at baseline (bottom) shows that the PSD increases at a broad-range of frequencies during ADs with a sharp peak in the delta frequency range. The solid lines represent the mean and the shading area between mean indicate SEM of data. n = 12 and 48 sessions for baseline and ADs, respectively, from 4 rats.
(C) Coherence analysis of the recordings from right and left BLA shows lack of evident coherence at baseline (left). In contrast, there is strong coherence during the two paroxysms of ADs in the delta frequencies (middle, the 30th session of stimulation in the third day of kindling, the animal reaching seizure stage 4). The magnifications are shown in black frames (right panels).
(D) Sample LFP and spectrograms with the kindling stimulation frequency set to 5 Hz (biphasic pulses at $\pm$270 μA). (E) Sample LFP and spectrograms with the kindling stimulation frequency set to 500 Hz (biphasic pulses at $\pm$ 200 μA).
(F) The elicited afterdischarges always show a very high and solitary PSD peak in the delta frequencies in a broad-band frequency of kindling simulations. The solid lines represent the mean and the color-filled area indicates the SEM of data numbers. n = 3 rats for 20, 50, and 100 Hz stimulation, n = 2 rats for 200 Hz stimulation, n = 1 rat for 5 and 500 Hz stimulation (it is hard to have ADT below 300 μA with the lowest 5 Hz and highest 200–500 Hz stimulation so that the n is smaller).

rhythms of the LFP (Figure 2A). Most interestingly, the delta oscillations are readily translated into behavioral manifestations (Figure 2D), namely, motor seizures or muscle convulsions tightly coherent with the LFP rhythms (Figure 2D). Essentially the absolute power of all frequency bands increases in seizures if compared with that in baseline (see also Figure 1B), with the delta power staying as the most prominent (~60% or more of the total power, Figure 2E). It is also interesting to note that from low-stage to high-stage seizures, the delta power does not show a marked increase but the absolute powers of the other frequency bands do (Figure 2E). The increase of the relative power of the other frequency bands is not as prominent, probably because delta power always constitutes >60% of the total power and there is a general increase in the absolute power in all of these "minor" bands (Figure 2F). On the other hand, the number of discharge units, overall firing rates, burst rates, and percentage of spikes in bursts of each unit all markedly increase with higher stages of seizures (Figure 2G).

The Increasing Discharges with Escalating Behavioral Seizures Are Phase-Locked to Delta Oscillations

We have seen that high-stage seizures are associated with increase in discharges and discharging units. We would further correlate the findings in MU with LFP recordings. The unit that shows evident discharges in low-stage seizures would have more discharges in high-stage seizures. Those which do not have discharges in low-stage seizures may show evident discharges in high-stage seizures (Figure 3A). In any case, the MU discharges in both low- and high-stage behavioral seizures tend to occur around the sink peak of LFPs (Figures 3B–3D) and be phase-locked to the delta oscillations in LFPs (Figure 3E). Despite that the spike numbers are increased in high-stage seizures, the phase-locking values are not significantly changed (Figure 3F), lending a strong support for the unchanged intrinsic frequency of network oscillations during the normal-ictal or interictal-ictal transitions and low-level seizures. The even more increase in single unit discharges in high-stage seizures may then be distributed to different frequency bands of the corresponding LFP recordings. The findings in Figures 2 and 3 indicate that the fundamental intrinsic rhythms are always observed even with the apparently much more chaotic summation of the local currents from the markedly increased cellular activities. The basic mechanism underlying kindling and initial epileptogenesis thus very likely involves more frequent discharges in more neurons, or more precisely, more burst discharges phase-locked to delta oscillations, which are readily translated into the same frequency-coded behavioral seizure manifestations.

Burst Discharges Appear Earlier and Last Longer in INs Than in PNs after Kindling Stimuli

We then turned to the slice preparations to further explore the cellular bases of the burst discharges and the intrinsic rhythms of BLA. Glutamatergic PNs and GABAergic INs in BLA slices can be identified morphologically and electrophysiologically (See Methods, Mahanty and Sah, 1998; Sah et al., 2003; Yang et al., 2020). Meanwhile, the spike frequency, especially the number of burst discharges, is markedly increased by kindling in both types of neurons especially in INs (Figure 4), well consistent with the increase in discharging units in Figure 2. Moreover, the burst discharges in adjacent INs and PNs are highly correlated. The burst discharges tend to be in phase at first, demonstrating an immediate common drive for PN and IN bursts provided by the kindling-like stimulation. The system, however, gradually moves into a pattern of reverberating discharges between PNs and INs in 20–30 s (when the burst discharges in PNs fade away), so that the burst discharges in INs correspond to the hyperpolarization rather than burst phase of PNs (Figures 4A and 4B). We would presume that the burst activities in reciprocally innervated PN and IN

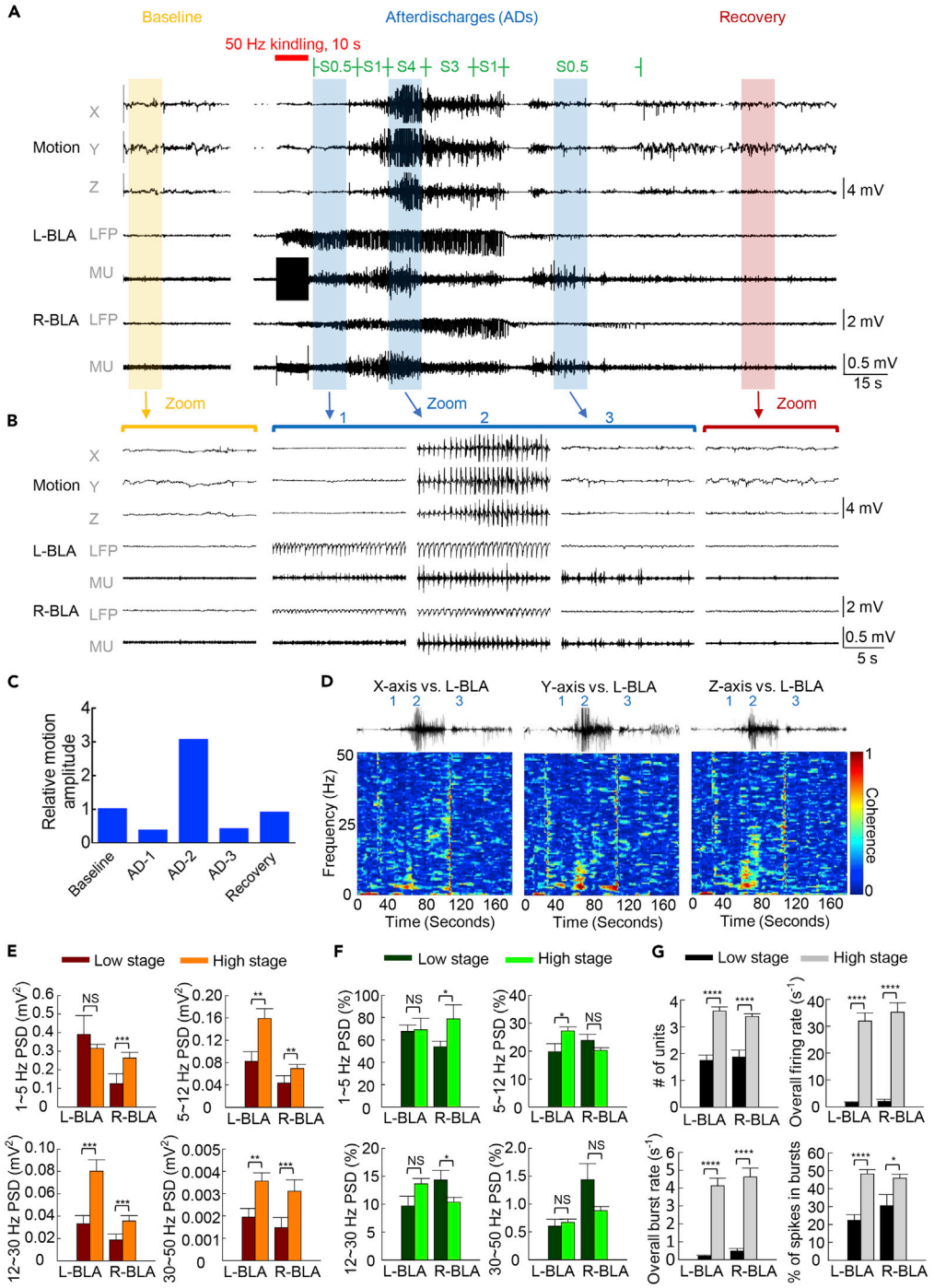

Figure 2. Number of Discharging Units and Power Are Increased with Aggravation of Behavioral Seizures

(A) Sample LFP and multi-unit (MU) tracings before and after the kindling stimulation (the first session in the first day, biphasic pulses at ±50 μA). The dynamic result of motion was detected from a 3-directional accelerometer simultaneously. Behaviorally the animal is in Racine stage 4 (seizures of higher stages would tend to give more MU discharges for analysis). Note the manifest MU discharges grouped into clusters roughly coinciding with the LFP changes after but not before the stimulation. The signals above LFP are also increased, and back to normal scale while the rat was recovered from seizure for ~2 min after kindling stimulation (zoomed figures in B). Also note that there are two paroxysms of afterdischarges, although the second one is much smaller than the first one and is more discernible in the MU than LFP recordings.

Figure 2. *Continued*

(B) Five 10-s enlargement figures show different behavioral states and corresponding recordings in a kindling session. The motion signal in baseline with fluctuant amplitude represents the slight walking movement of rat and became flat to indicate the pathologic still movement (absence-like) in the first zoomed figure of ADs after kindling stimulation. In the second figure of ADs, the motion signal of S4 was performed periodically in the similar rhythm with LFP, which indicates the tonic-clonic convulsion seizure of rat. The motion signal illustrates sluggish and slight rocking motion at the termination of seizure in the third figure of ADs, and returns to the normal waveform and represents the walking movement as baseline while recovery.

(C) The mean amplitudes were calculated from the area under curve of every 3-axis motion signals divided by time in (B) The ratio between the mean amplitude in each segment (AD-1, AD-2, AD-3, and recovery) and that at baseline is defined as the relative motion amplitude.

(D) Coherence analysis of the recordings from motion signals in 3-axis and left BLA LFP show strong coherency during the tonic-clonic seizure in the delta frequencies.

(E) The absolute powers of the delta (1–5 Hz) and the other frequency bands (5–12, 12–30, and 30–50 Hz) in the left and right BLA are compared between the low and high stages of seizures. Note the increase in power in the other frequencies than the delta band, which has by far the highest power in both seizure stages (note the different Y axis calibrations in different plots) (n = 16 epochs for low-stage and n = 40 epochs for high-stage seizures in 4 rats).

(F) The relative power (% total power) of the delta (1–5 Hz) and the other frequency bands (5–12, 12–30, and 30–50 Hz) in the left and right BLA are compared between the low and high stages of seizures. The database is the same as that in (E). Note that the delta power could constitute up to ~60%–80% of the total power in seizures. For the other frequency bands, the changes in relative power from low to high stage of seizures are apparently less remarkable than the absolute power in (E).

(G) The MU recordings for the epochs stably at the maximal behavioral seizures longer than 10 s are analyzed to show the marked increase in the number of discharge units, overall firing rates, burst rates, and percentage of spikes in bursts of each unit from low to high stages of seizures. n = 16 epochs for low-stage and n = 40 epochs for high-stage seizures in 4 rats.

Data are shown as means ± SEM. NS. $p > 0.05$, *$p < 0.05$, **$p < 0.01$, ***$p < 0.001$, ****$p < 0.0001$, Mann-Whitney U test.

would be mostly but not exactly out of phase. In other words, PN bursts would trigger IN bursts, which in turn terminate PN bursts. IN bursts require an enough drive from temporospatially summed PN activities, and thus would tend to develop late in PN bursts to make a relatively short overlap of the two bursts. IN bursts, however, would mostly correspond to the interburst intervals of PN, so that the PN is hyperpolarized and preconditioned for subsequent burst discharges upon the cessation of IN bursts. We also calculated the percentage of synchronized activities or events in different neuronal pairs (IN-IN, PN-PN, and PN-IN pairs, Figure 4C). We first specifically divided the post-kindling events into two categories, one including both burst discharges and EPSPs as both are excitatory and are similarly generated by excitatory synaptic inputs (Rainnie, 1999) and the other being IPSPs. In the 45-s period immediately after the 1-s stimulation, a very high percentage of bursts/EPSPs is synchronized in IN-IN and PN-PN pairs. Also, most of IPSPs are synchronized in PN-PN pairs and most of IPSPs in PN are synchronized with EPSPs in IN, consistent with the presumption that neighbor INs tend to fire synchronously to make an inhibitory "core" and recruit local clusters of PNs into a synchronized hyperpolarization phase. It is also of note that the burst discharges in INs tend to persist longer than those in PNs, and the burst discharges in PN are terminated rather abruptly upon the start of the burst discharges in INs, well consistent with the different propensity for burst discharges and especially the different inhibitory "tone" on PNs and INs in the system (see Introduction and Discussion).

The IN-PN Burst Discharges Define an Oscillation Frequency in the Delta Range

We have seen that kindling markedly increases cellular activities, especially burst discharges in both *in vivo* and *in vitro* studies (Figures 2, 3, and 4). Figure 5 further shows that the increase in discharges could usually last for ~40–50 s in INs but quite shorter in PNs. Moreover, it seems that the repetitive burst discharges have a relatively fixed burst duration and more variable interburst interval (Figures 5A and 5B). The burst duration has a mean of ~0.5 s immediately after kindling in both PNs and INs and shows just very small or negligible changes within the next ~20–40 s. The interburst interval, on the other hand, tends to be short (~0.5–1 s) right after kindling and then gets longer and longer to ~1.5–3 s before the bursts cease to happen. The sum of the burst duration and the interburst interval then could readily make a wavelength as short as ~1 s. This is a figure at room temperature. The wavelength could be shorter *in vivo*, and therefore well compatible with the prevalent delta oscillations in Figures 1, 2, and 3. It is then plausible that the cellular basis of delta-range intrinsic rhythms in normal, post-kindling ADs, and seizure discharges could be ascribed to burst discharges, which would potentially give rise to a large current flow and consequently a

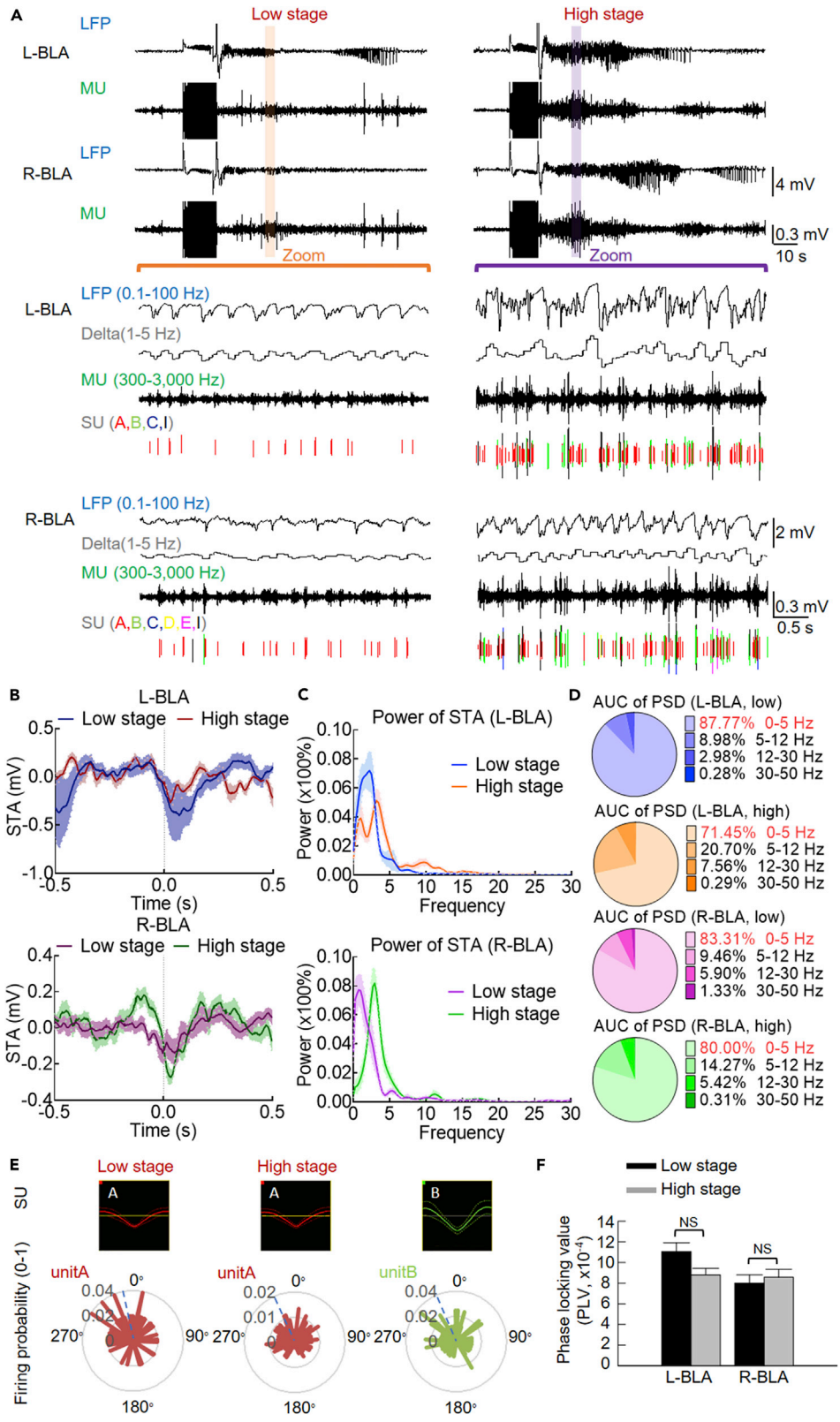
A
Low stage
High stage
LFP
L-BLA
MU
LFP
R-BLA
MU
4 mV
0.3 mV
10 s
Zoom
Zoom
L-BLA
LFP (0.1-100 Hz)
Delta(1-5 Hz)
MU (300-3,000 Hz)
SU (A,B,C,I)
R-BLA
LFP (0.1-100 Hz)
Delta(1-5 Hz)
MU (300-3,000 Hz)
SU (A,B,C,D,E,I)
2 mV
0.3 mV
0.5 s
B
L-BLA
Low stage
High stage
STA (mV)
Time (s)
R-BLA
Low stage
High stage
STA (mV)
Time (s)
C
Power of STA (L-BLA)
Low stage
High stage
Power (x100%)
Frequency
Power of STA (R-BLA)
Low stage
High stage
Power (x100%)
Frequency
D
AUC of PSD (L-BLA, low)
87.77% 0-5 Hz
8.98% 5-12 Hz
2.98% 12-30 Hz
0.28% 30-50 Hz
AUC of PSD (L-BLA, high)
71.45% 0-5 Hz
20.70% 5-12 Hz
7.56% 12-30 Hz
0.29% 30-50 Hz
AUC of PSD (R-BLA, low)
83.31% 0-5 Hz
9.46% 5-12 Hz
5.90% 12-30 Hz
1.33% 30-50 Hz
AUC of PSD (R-BLA, high)
80.00% 0-5 Hz
14.27% 5-12 Hz
5.42% 12-30 Hz
0.31% 30-50 Hz
E
Low stage
High stage
SU
Firing probability (0-1)
unitA
unitA
unitB
F
Low stage
High stage
Phase locking value (PLV, x10⁻⁴)
NS
NS
L-BLA
R-BLA

Figure 3. The Single-Unit Discharges in Burst Are Increased and Phase-Locked to Delta Oscillations in Both Low and High Stages of Behavioral Seizures

(A) Sample sweeps are collected for the LFP (band pass filtering at 0.1–100 Hz), LFP for the delta range frequency (band pass filtering at 1–5 Hz), MU (band pass filtering at 300–3000 Hz), and sorted SU from the MU, during low and high stages of seizures (Racine stage 1 and 5, in the second stimulation session in the first day and the fifth stimulation session in the third day, respectively, biphasic pulse at ± 170 μA in the same rat). The sorted different SU of discharges are shown in different colors (see Methods for the sorting criteria). Note the increase of higher-frequency oscillations in LFP recordings during the high-stage seizures.

(B) Spike-triggered average (STA) of ADs in both low and high behavioral seizure stages in bilateral BLAs were demonstrated. The spike's timestamp of a single unit was taken as a reference, and the 1-s waveforms of LFPs nearby the spikes (0.5 s on each side) were averaged.

(C) Power spectrum analysis of the STA in (B) reveals several oscillatory cycles at the delta frequencies around the spikes. The solid lines represent the mean, and the shaded area between the mean indicate SEM of data. n = 11 and 22 units in 4 rats for the low-stage and high-stage seizures in L-BLA, and n = 11 and 15 units in 4 rats for the low-stage and high-stage seizures in R-BLA in both (B) and (C).

(D) Pie charts represent the percentage area under the PSD curves of each frequency band in (C).

(E) Top: waveforms of the SU in (A). Unit A is already present during the low-stage seizures and markedly increases in firing rate in the high-stage seizures. Note the lack of significant changes in its configuration or waveform (left two panels). On the other hand, unit B is present only in high-stage seizures. Bottom: Sample polar plots of the firing probability within the delta cycle of discharging units in the upper panel. The measurement of phase lock is shown by polar plots, which consist of probability (the number beside the inner circle) and phase angle (the number beside the outer circle). The length and direction of the bar "vectors" are depicted to show the probability of discharges happening at specific phase angles (e.g., bars touching the outer circle would indicate a higher probability than that touching the inner circle). All bar vectors are averaged to make a mean resultant vector, whose direction is shown by the dashed line. It is of note that the dotted line is always close to the zero degree, well consistent with the result of STA in (B)–(D), where the nadir is roughly at time point zero.

(F) Only the units that are present in both low and high stages of seizures (e.g., unit A in E) were calculated for the comparison of phase locking values (PLVs). Cumulative results are shown in the right panel, demonstrating the very similar PLVs in the low- and high-stage seizures in the left (n = 13 epochs and 45 epochs for the low and high stages of seizures in 7 units, 4 rats, respectively) and right BLA (n = 11 epochs and 39 epochs for the low and high stages of seizures in 7 units, 4 rats, respectively). It is evident that the discharges of the unit increase a lot during high-stage seizures, but the phase-locking value (PLV) remains roughly the same.

Data are shown as means ± SEM. NS. $p > 0.05$. Mann-Whitney U test.

large change in local field potential. In this regard, the relatively fixed duration of the bursts in both PNs and INs may further implicate the well-orchestrated intrinsic and extrinsic currents to end the bursts. The more variable or gradually lengthened interburst interval, on the other hand, may signal fading of the effect of kindling stimulation and thus a decrease in propensity for burst generation.

Enhancement of Synchrony Precedes Increase of Discharges to Determine Seizure Staging

We have seen that high-stage seizures are associated with more frequent of neuronal (burst) discharges (Figures 2 and 3) and that kindling has dual effects, increasing and synchronizing neuronal (burst) discharges (Figures 4 and 5). We therefore endeavor to dissect the causal relation among synchronization and increase of neural activities and behavioral seizures in more detail. Consistent with the findings in Figure 2, the ADs typically wax and wane and are associated with different behavioral stages of seizures. Also, more single unit activities are associated with higher level of synchronization and behavioral seizure staging (Figure 6A). Interestingly, the level of synchronization also tends to "oscillate" at delta frequencies during the periods of high-stage behavior seizures (Figure 6B), implicating that the delta oscillations in LFP are based on the synchronized unit discharges and thus summed local currents. Also, enhancement of synchronization is always documented before the escalation of discharge numbers and seizure staging, whereas declination of synchronization is noted after decrease of discharges and seizure staging (Figure 6C). These findings strongly implicate that enhanced synchronization constitutes the base for the substantial increase of discharges and behavioral manifestations of seizures. In this regard, behavioral seizures could apparently wane with decreased discharges but may wax again if the level of synchronization still sustains. Seizures would be "truly" ceased after the level of synchronization truly declines.

Delta Oscillations Take ~2 s to Happen but Are Responsible for Distant Spreading

If the enhanced synchrony in the delta bands finally leads to highly coherent behavioral manifestations (Figures 2 and 6), could the transmission happen en route of the telencephalic pathways? Taking advantage of the lack of noise associated with optical stimuli, we recorded the LFP in bilateral BLA, thalamic mediodorsal

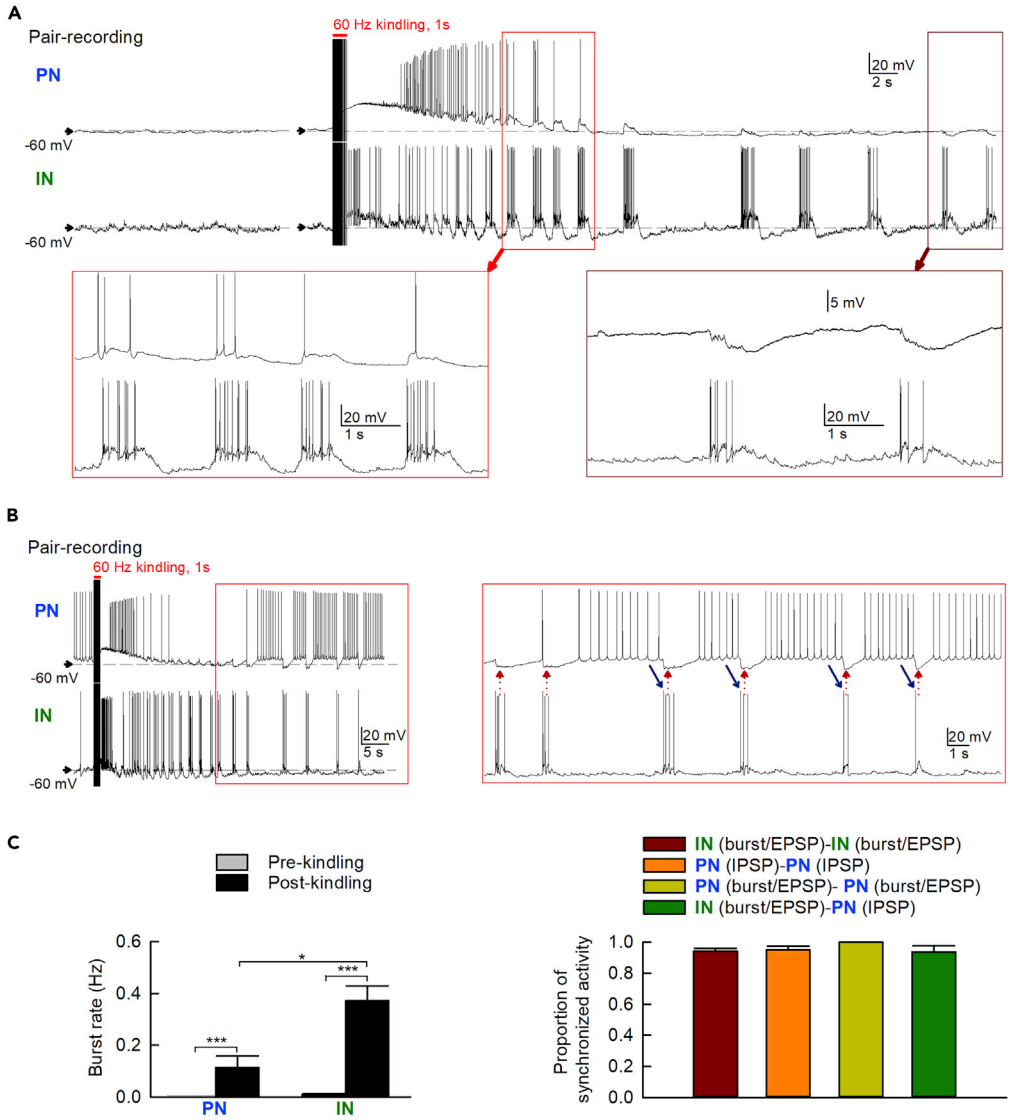

Figure 4. IN and PN Both Show a Marked Increase in Burst Discharges after Kindling-like Stimulation

(A) Representative pair recordings of a PN (top) and an IN (bottom) showing the kindling-induced discharges. The kindling-induced postsynaptic events in the PN are characterized by burst discharges with gradual transition into EPSPs and then IPSPs. In the IN, kindling-like stimulation induces repetitive burst discharges that typically last longer and are coupled to the burst discharges, EPSPs, or IPSPs in the PN (see boxes for a closer view of the traces).

(B) Another representative pair recording shows alternating discharges between PN and IN, particularly toward in the later phase of the post-kindling period (see boxes for a closer view of the traces). Note that the small perturbations in the membrane potential immediately before the bursts in IN could be roughly correlated with the spikes in the bursts in PN (blue arrows). Also, the termination of the bursts in PN is much more abrupt than the onset and is exactly synchronized with the onset of the burst discharges in IN.

(C) Left: Kindling-like stimulation induces a marked increase in burst discharges in both PNs and INs, especially in the latter (n=10 and 17 for PNs and INs, respectively). Right: Analyses of the proportion of synchronized activities in different neuronal pairs (IN-IN, PN-PN, and PN-IN) show that nearly all post-stimulation postsynaptic events are synchronized. Post-stimulation activities are defined as "synchronized" when the onset times of any two postsynaptic events (burst, EPSP, and IPSP), respectively, in the two neurons in a pair-recording differ by no more than 50 ms. The brown bar denotes the proportion of synchronous bursts and/or EPSPs in all post-stimulation bursts and EPSPs (484 events in total) in IN-IN pairs (n = 8 pairs from 8 mice). The orange bar denotes the proportion of synchronous IPSPs in all post-stimulation IPSPs (223 IPSPs in total) in PN-PN pairs (n = 8 pairs from 8 mice). The olive bar denotes the proportion of synchronous bursts and/or EPSPs in all post-stimulation bursts and EPSPs (52 events in total) in PN-PN pairs (n = 8 pairs from 8 mice). The green bar denotes the proportion of IPSPs in PN that is synchronized with EPSPs in IN in all post-kindling PN IPSPs (total of

Figure 4. *Continued*
150 IPSPs) in PN-IN pairs (n = 8 pairs from 8 mice). The burst rates and numbers of synchronous events were analyzed in a 45-s period before and/or after each stimulation.
Data are shown as means ± SEM. *p < 0.05, ***p < 0.001, Mann-Whitney U test or Wilcoxon signed-rank test.

nuclei, and prelimbic cortices before, during, and immediately after a 10-s optogenetic stimulation of PN in the left BLA. It is evident that vivid delta oscillations start at 2–3 s after the initiation of light stimulation in the left BLA and readily spread to all of the other five structures at roughly the same time or slightly later (~4 s) after light initiation. In the meanwhile, gradual increment in delta power is noted in all of the six structures. The power stays rather high thereafter, with synchronous fluctuations in the six structures (Figure 7A). The time courses of phase angle changes in the other five structures are in general very similar to or synchronized with those in the left BLA during and after but not before the onset of vivid delta oscillations elicited by the light stimulation (Figures 7B–7D). Consistently, the coefficients of determination between left BLA and each of the other five structures are low at the beginning of light stimulation, reaching a similar high level both during and immediately after the delta wave start to spread, and then becoming somewhat fluctuating (Figures 7B–7D). The reverberating burst discharges in IN and PN and consequent delta oscillations in BLA thus could play a key role not only in epileptogenesis, or generation of an abnormal focus of self-sustaining reverberating discharges, but also in seizure spreading, or transmission of the abnormal activities to the other key brain structures (Figure 7E). An intrinsic rhythm in the delta band then is likely a fundamental feature of corticothalamic oscillation system, including the ancient amygdalohippocampal complexes.

DISCUSSION

Enhanced Synchronization Plays a More Fundamental Role Than Excessive Discharges in Ictogenesis

It is a common concept that epileptic seizures are characterized by excessive and synchronized neuronal activities (Stafstrom, 1998). Consistently, we have shown that the behavioral staging of seizures is closely correlated with number of discharges and discharging units (Figures 2 and 3). Kindling-like stimulation also elicits synchronized burst discharges in both PN and IN (Figure 4). Most interestingly, the changes in synchrony in bilateral BLA also oscillate in delta frequencies and always precede and outlast the changes in discharging units as well as behaviors (Figure 6). Increase and decrease of synchronization therefore seem to be the most fundamental attributes characterizing seizure onset and offset. BLA contains glutamatergic PNs as well as a relatively smaller number of GABAergic INs. Despite the extensive glutamatergic connections between PNs (Smith and Paré, 1994), the spontaneous firing rates of PNs are usually very low (<1 Hz), presumably ascribable to the abundance of inhibitory synapses at the soma and proximal processes of PNs (McDonald and Betette, 2001). Consistently, the membrane potential of PNs is dominated by frequent inhibitory postsynaptic potentials (IPSPs) contributed by INs (Paré et al., 2003). These findings imply stronger baseline activities in INs than in PNs, which may also be partly ascribable to the fact that INs are interconnected by both dendritic and axo-axonic gap junctions in terminals (Muller et al., 2005; Woodruff and Sah, 2007b). Large populations of INs may thus fire synchronously with millisecond precision (Hestrin and Galaretta, 2005) to make an inhibitory "core," which may then recruit local clusters of PNs into a synchronized hyperpolarization phase and precondition the PNs for subsequent burst discharges (Ariniadou-Anderjaska et al., 2018; Ohshiro et al., 2011). Accordingly, burst discharges are more readily observed in INs than in PNs (Figures 4 and 5), supporting the basic role of INs in the synchronization of network activities (Woodruff and Sah, 2007a). The apparent neural activities (excessive discharges) and temporospatial involvement of the oscillations (seizure staging) could then be closely related or even consequential to the level of synchronization of the convergent inputs into a neuron, IN and especially PN. It would be desirable to further explore the molecular and cellular mechanisms of the modulation (increase/decrease) of synchronization, which is very likely the most central issue of epileptogenesis and ictogenesis, and probably even neural computations underlying normal cognitive processes considering the same major frequency band of oscillations in normal and seizure conditions (Figure 1).

Alternate Burst Discharges in PNs and INs Set the Intrinsic Rhythms of BLA and Relevant Telencephalic Networks

We have seen that BLA has a delta-range intrinsic rhythm (or natural frequency) of oscillation in either normal or seizure conditions (Figures 1 and 2). The high-fidelity phase lock of burst discharges to the delta-range LFP oscillations (Figure 3) and the ~2-Hz fluctuation of the synchronization (or similarity) score

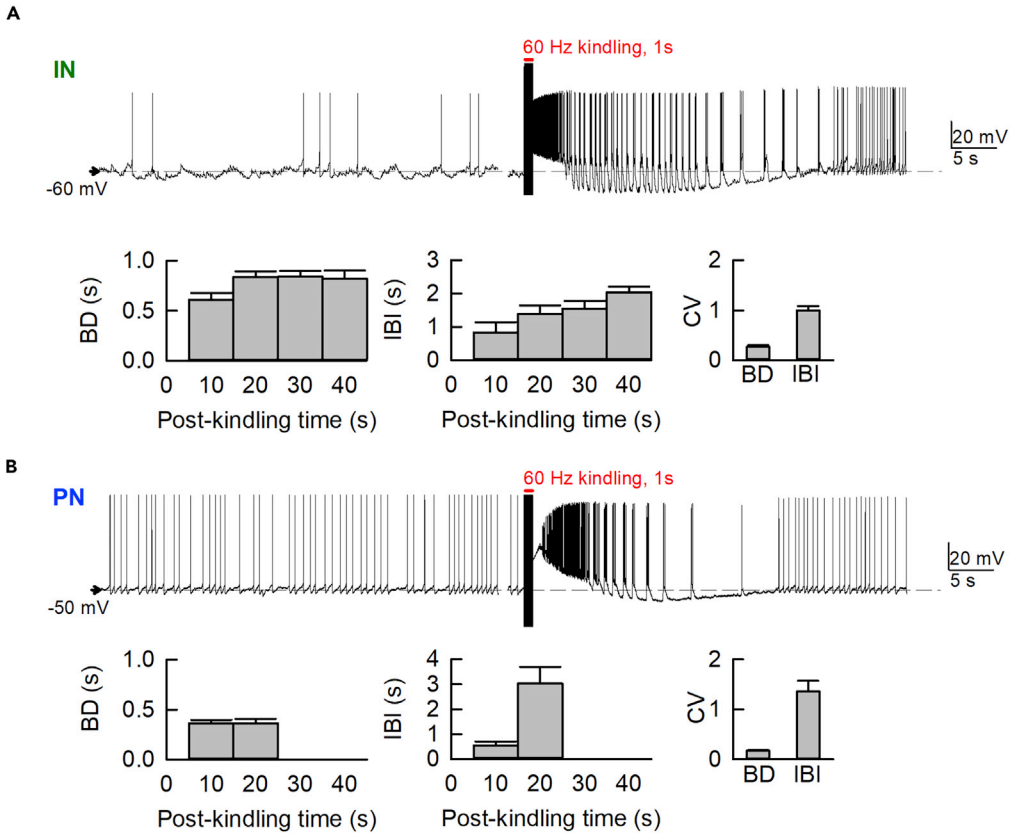

Figure 5. Kindling Stimulation Induces Recurrent Discharges with a Wavelength of Roughly 1–2 s

Kindling-like stimulation triggers burst discharges in INs (A, top) and PNs (B, top). The duration of burst discharges (BD) is more fixed than the interburst interval (IBI), which tends to be gradually lengthened toward the late phase after kindling before the burst discharges finally cease to happen (or are turned into spike mode of discharges). The coefficient of variation (CV) is therefore very low for BD but much higher for IBI in both INs and PNs. Note that immediately after the kindling-like stimulation, there could be a plateau depolarization phase, which may mimic paroxysmal or sustained depolarization in seizure discharges and be superimposed with dense spikes in either IN or PN. We therefore choose to start the analysis of BD and IBI 5 s after the kindling-like stimulation, so that the probable effect of post-kindling plateau depolarization may be minimized. BD and IBI are averaged in 10-s intervals between 5–45 s (for INs) or 5–25 s (for PNs). The period of analysis is shorter for PNs whose kindling-induced burst discharges tend to be less persistent than that in IN (each n = 4). Data are shown as means ± SEM.

of single unit discharges during behavioral seizures (Figure 6) further implicate that this major rhythm in LFP is ascribable to time-dependent changes in summed local currents due to bursts repeating in similar frequencies. Accordingly, kindling induces alternating bursts in INs and PNs, and the "wavelength" set by burst duration and interburst interval is compatible with delta oscillations (Figures 4 and 5). From a single neuron's perspective, the cellular burst discharges themselves in seizures may be qualitatively similar to that in normal conditions. The key changes associated with seizures are thus more in the network than in the cellular level. Consistently, there is a more variable interburst interval (presumably more influenced by extrinsic network inputs) than burst duration (presumably more determined by intrinsic cellular properties) in Figure 5. The variability in burst duration and especially the interburst interval could then serve as part of the mechanism underlying the changes in predominant frequencies during the evolution of epileptic seizures (Beenhakker and Huguenard, 2009; Steriade and Amzica, 2003). Constraints of the major frequency modulation to a common (delta) band may have an imperative benefit in information flow, namely, a prompt spatial spreading or temporal re-entry in different telencephalic structures (Figure 7, also see below), although it could be at an expense of limitations on data coding/decoding in the frequency domain. In any case, information relay in BLA and relevant telencephalic structures may therefore rely more on the time and the spatial domains, probably an evolutionarily more advanced rationale of

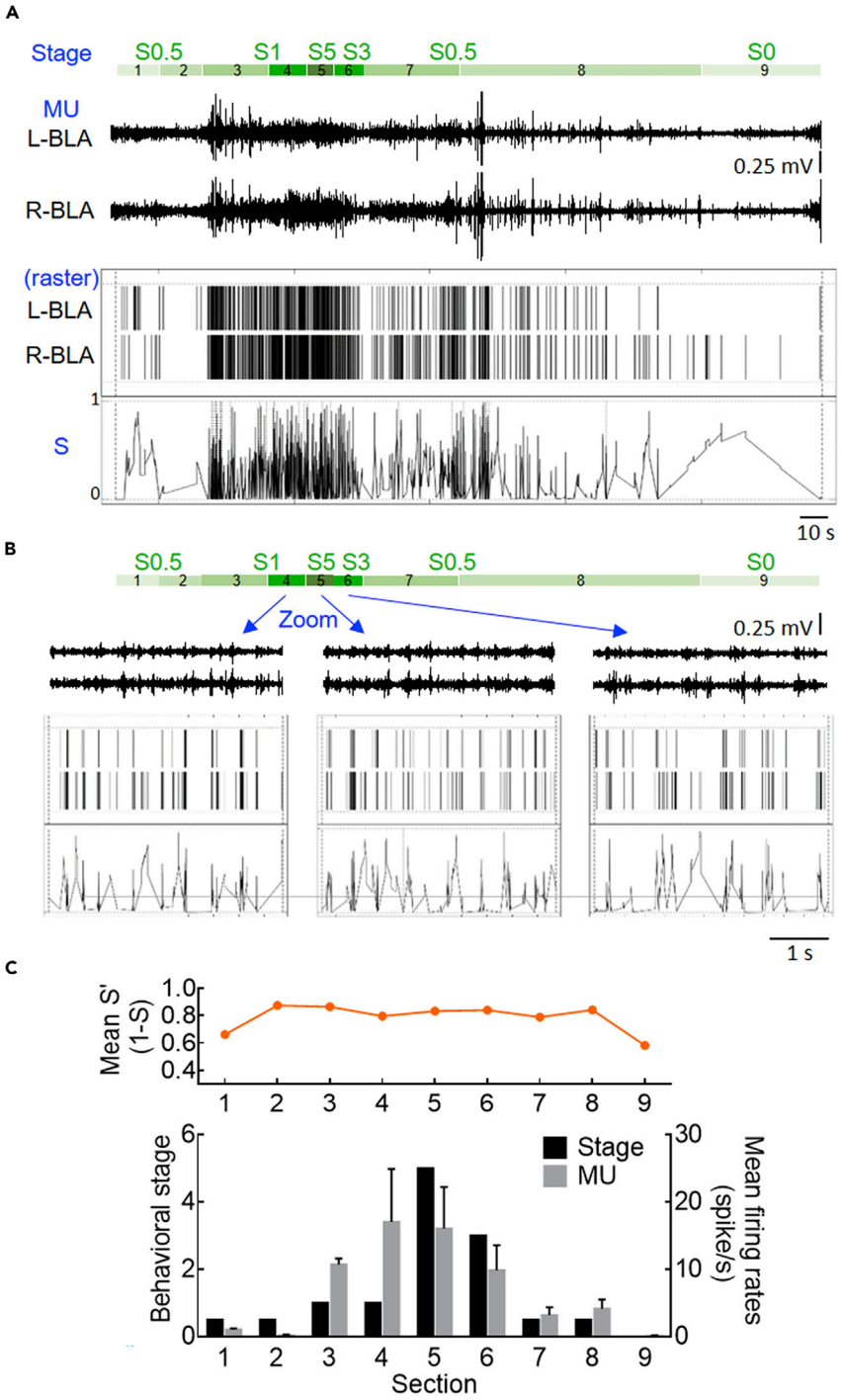

Figure 6. Synchronization of Multi-Unit Activities Increases before and Decreases after Corresponding Changes in Discharge Rates and Behavioral Seizures

(A) Top: Corresponding to the recordings, behavioral seizure stages are gradually increased to reach the maximum (S5) and then gradually attenuated. Note that at low-stage (S0.5 – S1) seizures, the behaviors are coded into different colored segments if the rat has a large-enough movement to change its posture (probably implicating a significant change in electrophysiological activities) but remains in the same seizure stage according to Racines criteria. Lower: Sample multi-unit spikes (MU) and the rasters from the ADs in bilateral BLA after a ±270 μA stimulus (the ninth session of kindling procedure). The dissimilarity profiles are calculated from SPIKY (see Methods). S is the dissimilarity score, with 0 for complete synchrony and 1 for complete asynchrony between the two spike trains.

Figure 6. *Continued*

(B) A closer view of the data in (A) at the highest-stage (S5) and the adjacent segments shows that the dissimilarity profile also oscillates roughly at the delta frequency range around a mean level of ~0.178.

(C) The mean similarity score (S′, derived from 1-S to have a more straightforward correlation with the level of synchronization) is plotted on top of the simultaneous mean multi-unit firing rates (spike frequency) in bilateral BLA and the seizure stage in each segment of behavioral seizures. Note the close correlation between the firing rate and seizure stage. The level of synchronization, however, increases before and decreases after the corresponding changes in firing rates and behavioral seizures.

Data are shown as means ± SEM.

neural computation in a more developed and complicated system that preserves similar IN-PN network and thus similar basic intrinsic rhythms of the oscillating activities.

Reverberating Delta Oscillations May Be Faithfully Relayed Distantly to Result in Coherent Behavioral Seizures

We have seen that, at least in mild convulsive seizures, muscle contractions could happen in delta frequencies strictly coherent to the oscillations in concomitant LFP recordings (Figure 2B). This is partly analogous to a well-known phenomenon that myoclonic jerks or clonic convulsions may be observed concurrently with the burst-suppression patterns in electroencephalograms (EEGs) (Hamer et al., 1999, 2003), where bursts of high-voltage local field potentials alternate with an attenuated or suppressed background. The regularly recurring behavioral manifestations well correlative to the concomitant rhythmic LFP therefore is rather distinctive and strongly implicates the involvement of excitation-inhibition cycles in delta rhythms (Figure 2D), very much consistent with the findings in Figures 4 and 5. The highly coherent behavioral manifestations also lend a strong support for the imperativeness of delta oscillations, which serve as the basic or natural frequencies of the telencephalic networks. It is of note that MD, prelimbic cortex, and contralateral BLA (Figure 7) are all telencephalic structures receiving direct glutamatergic input from left BLA (McDonald, 1987, Mátyás et al., 2014, Hintiryan et al., 2019; Huang et al., 2019; Hsu et al., 2020). In contrast to the potential role of INs in local spreading (see above), PN probably is essential for distant or long-range projection of the oscillating activities. Although the resonance among different structures and corresponding behavioral consequences are well demonstrated, there are different scenarios. There could be no evident limb convulsions in lower-stage (e.g., stages 1–2) seizures where delta oscillations are already present. The synchronization or resonance among different telencephalic structures therefore is not necessarily associated with vivid behavioral translations. It would be desirable to see whether the temporospatial extent of macroscopic involvement and the microscopic distribution of the burst discharges between segregation and transmission coding (Akam and Kullmann, 2014; Eggermont and Smith, 1996; Krahe and Gabbiani, 2004) could play an important role in the "motor execution" under such circumstances. In any case, it is plausible that the impulses from different re-entrant pathways with the expanding seizure network might collide to result in desynchronization. This may probably be considered as a reason why most clinical seizures would usually stop by themselves. Effective therapies for seizures, then, should not be simplistically based on increased inhibition or decreased excitation but more comprehensively on curtailing the pathologically augmented resonating oscillations back to normal.

Limitations of the Study

We endeavored to correlate *in vitro* and *in vivo* findings to decipher the cellular basis of oscillating network activities and behavior seizures. Although we have deliberately performed the stimulation and recordings chiefly in the basolateral amygdala (BLA), the reduced preparation of brain slices and the temperature differences between *in vivo* and *in vitro* conditions may interfere with a fully quantitative and exact correlative argument. The wavelength of the oscillation is ~1 s if set by the sum of *in vitro* burst and interburst intervals. This figure corresponds to a frequency of ~1 Hz, modestly slower than the 2–3 Hz oscillations in *in vivo* recordings that are performed in higher temperatures. We would still presume a basic consistency between the *in vitro* and *in vivo* data, with explicit discussion of the potential limitation in the paper.

Resource Availability

Lead Contact

Further information and requests for resources and reagents should be directed to and will be fulfilled by the Lead Contact, Ya-Chin Yang (ycyang@mail.cgu.edu.tw).

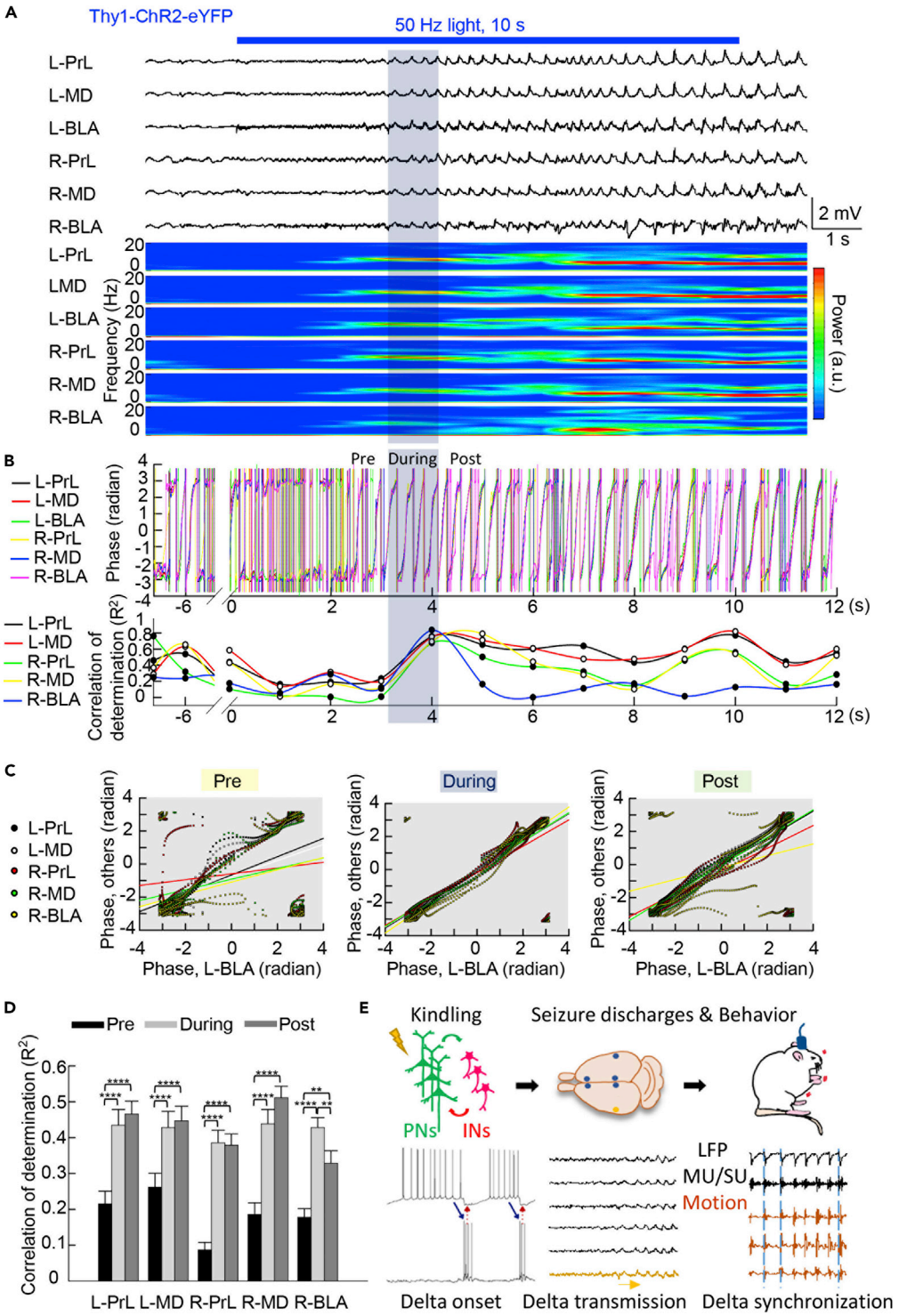

Figure 7. Delta Oscillations Take ~2 s to Happen and Are Readily Spread to Distant Brain Structures

(A) Simultaneous LFP recordings are obtained from bilateral BLA, thalamic mediodorsal nuclei (MD, posterior 1.5 mm, lateral 0.4 mm, and deep 3.25 mm relative to bregma in mice) and prelimbic cortices (PrL, anterior 2 mm, lateral 0.4 mm, and deep 2.75 mm relative to bregma in mice) before, during, and immediately after a 10-s optogenetic stimulation (optokindling) of the left BLA in the Thy1-ChR2-eYFP mice (6 mW, 1 ms, 50 Hz × 10 s, the first stimulation session on the first day, behaviorally Racine stage 1). Delta oscillations in left BLA and/or the other structures are discernible 2–3 s after

Figure 7. *Continued*

the onset of the optogenetic stimulation. The delta oscillations in all of the six structures start to reach the maximal synchrony at 4.08 ± 0.22 s (please refer to Methods for the determination of the starting point of maximal phase synchronization, n = 30 kindling sessions in 2 mice) after the onset of stimulation of left BLA. Concomitant time frequency analysis shows gradual increment in delta power in all of the six structures in the first 2–3 s and apparently changes in the high delta power zones thereafter. The phase difference is calculated between any two of the six electrodes and averaged for each time point. The first point of 100 consecutive points for which the square of the average is below 0.25 Rad^2 is defined as the starting point of maximal phase synchronization. The 1-s period right before the starting point of maximal phase synchronization is marked "pre." From this point on, a 1-s period is marked "during" (the shaded area) and the following 1-s period is marked "post" (see B).

(B) The three 1-s periods in (A) were taken for further analysis. The instantaneous phase angle of the delta band oscillations in (A) is calculated based on Hilbert transform; only the phase components are extracted and the amplitude components are left out. The instantaneous phase angle is then plotted against the time elapsed after the start of light stimulation (designated as time point 0), demonstrating the very high phase synchronization among the six structures during and even after, but not before, the 1-s shaded zone (upper panel). The coefficient of determination (R^2) between the delta band oscillation in left BLA and in each of the other five structures is calculated and plotted against the time elapsed, showing the extremely congruent R^2 between each of the five structures and left BLA during the shaded zone (lower panel).

(C) The instantaneous phase angle in each of the other five structures is plotted against that in the left BLA (bottom) for three consecutive segments of time, namely, the 1-s period immediately before the shaded zone (pre), the 1-s shaded zone itself ("during"), and the 1-s period immediately after the shaded zone ("post"). The phase angles vary a lot before the shaded zone ("pre") but are very congruent between any one of the five structures and left BLA during and even after the shaded zone ("post").

(D) R^2 is calculated for the foregoing three 1-s periods. It is evident that R^2 between each of the other five structures and left BLA is much lower before ("pre") than that during and after ("post") the shaded zone (i.e., the onset of delta synchronization). n = 30 epochs in 2 mice. Data are shown as means ± SEM. *p < 0.05, **p < 0.01,***p < 0.001, ****p < 0.0001, Wilcoxon signed rank test.

(E) A brief summary and a probable mechanistic orchestration for further evaluation: BLA kindling could readily induce seizure discharges oscillating in delta frequencies in local field recordings, with the phase-locked single and multi-unit activities. The augmented delta oscillations could readily transmit to the other telencephalic structures as if different tuning forks resonate in their common natural frequencies and even lead to tightly correlated behavioral manifestations.

Materials Availability

This study did not generate new unique reagents.

Data and Code Availability

The data supporting the current study have not been deposited in a public repository but are available from the corresponding author on request.

The code is available at https://github.com/PingChou0207/2020_Delta-synchronization.

METHODS

All methods can be found in the accompanying Transparent Methods supplemental file.

SUPPLEMENTAL INFORMATION

Supplemental Information can be found online at https://doi.org/10.1016/j.isci.2020.101666.

ACKNOWLEDGMENTS

The authors are grateful to the Neuroscience Research Center of Chang Gung Memorial Hospital, Linkou, Taiwan. This work was supported by Grants MOST107-2311-B-182-004 (to Y.-C.Y.), MOST108-2311-B-182-001 (to Y.-C.Y.), MOST109-2320-B-182-006 (to Y.-C.Y.), MOST106-2320-B-002-014-MY3 (to C.-C.K.), MOST 106-2321-B-002 -032 (to C.-C.K.), MOST107-2321-B-002-012 (to C.-C.K.), MOST108-2321-B-002-007 (to C.-C.K.), and MOST109-2326-B-002-001 (to C.-C.K.) from Ministry of Science and Technology, Taiwan, and Grants CMRPD1H0091-3 (to Y.-C.Y.) from Chang Gung Medical Foundation, Taiwan. The graphical abstract is created with biorender.com

AUTHOR CONTRIBUTIONS

P.C., G.-H.W., and S.-W.H. conducted the experiments. P.C., G.-H.W., Y.-C.Y., and C.-C.K. analyzed the data and wrote the manuscript. Y.-C.Y. and C.-C.K. conceived the study and supervised the research.

DECLARATION OF INTERESTS

The authors declare no competing interests.

Received: June 16, 2020
Revised: September 9, 2020
Accepted: October 7, 2020
Published: November 20, 2020

REFERENCES

Akam, T., and Kullmann, D.M. (2014). Oscillatory multiplexing of population codes for selective communication in the mammalian brain. Nat. Rev. Neurosci. *15*, 111–122.

Ali, I., O'Brien, P., Kumar, G., Zheng, T., Jones, N.C., Pinault, D., French, C., Morris, M.J., Salzberg, M.R., and O'Brien, T.J. (2013). Enduring effects of early life stress on firing patterns of hippocampal and thalamocortical neurons in rats: implications for limbic epilepsy. PLoS One *8*, e66962.

Aroniadou-Anderjaska, V., Pidoplichko, V.I., Figueiredo, T.H., and Braga, M.F.M. (2018). Oscillatory synchronous inhibition in the basolateral amygdala and its primary dependence on NR2A-containing NMDA receptors. Neuroscience *373*, 145–158.

Beenhakker, M.P., and Huguenard, J.R. (2009). Neurons that fire together also conspire together: is normal sleep circuitry hijacked to generate epilepsy? Neuron *62*, 612–632.

Capogna, M. (2014). GABAergic cell type diversity in the basolateral amygdala. Curr. Opin. Neurobiol. *26*, 110–116.

Connors, B.W., and Gutnick, M.J. (1990). Intrinsic firing patterns of diverse neocortical neurons. Trends Neurosci. *13*, 99–104.

Eggermont, J.J., and Smith, G.M. (1996). Burst-firing sharpens frequency-tuning in primary auditory cortex. Neuroreport *7*, 753–757.

Faught, E., Kuzniecky, R.I., and Hurst, D.C.J.E. (1992). Ictal EEG wave forms from epidural electrodes predictive of seizure control after temporal lobectomy. Electroencephalogr. Clin. Neurophysiol. *83*, 229–235.

French, J.D., Gernandt, B.E., and Livingston, R.B. (1956). Regional differences in seizure susceptibility in monkey cortex. AMA Arch. Neurol. Psychiatry *75*, 260–274.

Goddard, G.V., McIntyre, D.C., and Leech, C.K. (1969). A permanent change in brain function resulting from daily electrical stimulation. Exp. Neurol. *25*, 295–330.

Hamer, H.M., Lüders, H.O., Knake, S., Fritsch, B., Oertel, W.H., and Rosenow, F. (2003). Electrophysiology of focal clonic seizures in humans: a study using subdural and depth electrodes. Brain *126*, 547–555.

Hamer, H.M., Wyllie, E., Luders, H.O., Kotagal, P., and Acharya, J. (1999). Symptomatology of epileptic seizures in the first three years of life. Epilepsia *40*, 837–844.

Hestrin, S., and Galarreta, M. (2005). Electrical synapses define networks of neocortical GABAergic neurons. Trends Neurosci. *28*, 304–309.

Hintiryan, H., Bowman, I., Johnson, D.L., Korobkova, L., Zhu, M., Khanjani, N., Gou, L., Gao, L., Yamashita, S., Bienkowski, M.S., et al. (2019). Connectivity characterization of the mouse basolateral amygdalar complex. bioRxiv, 807743, https://doi.org/10.1101/807743.

Hsu, T.T., Huanf, T.N., and Hsueh, Y.P. (2020). Anterior commissure regulates neuronal activity of amygdalae and influences locomotor activity, social interaction and fear memory in mice. Front. Mol. Neurosci. *13*, 47.

Huang, T.N., Hsu, T.T., Lin, M.H., Chuang, H.C., Hu, H.T., Sun, C.P., Tao, M.H., Lin, J.Y., and Hsueh, Y.P. (2019). Interhemispheric connectivity potentiates the basolateral amygdalae and regulates social interaction and memory. Cell Rep. *29*, 34–48.e34.

Jalilifar, M., Yadollahpour, A., Moazedi, A.A., and Ghotbeddin, Z. (2016). Classifying amygdala kindling stages using quantitative assessments of extracellular recording of EEG in rats. Brain Res. Bull. *127*, 148–155.

Jefferys, J.G., de La Prida, L.M., Wendling, F., Bragin, A., Avoli, M., Timofeev, I., and Lopes da Silva, F.H. (2012). Mechanisms of physiological and epileptic HFO generation. Prog. Neurobiol. *98*, 250–264.

Krahe, R., and Gabbiani, F. (2004). Burst firing in sensory systems. Nat. Rev. Neurosci. *5*, 13–23.

Lang, E.J., and Paré, D. (1998). Synaptic responsiveness of interneurons of the cat lateral amygdaloid nucleus. Neuroscience *83*, 877–889.

Lisman, J.E. (1997). Bursts as a unit of neural information: making unreliable synapses reliable. Trends Neurosci. *20*, 38–43.

Mátyás, F., Lee, J., Shin, H.S., and Acsády, L. (2014). The fear circuit of the mouse forebrain: connections between the mediodorsal thalamus, frontal cortices and basolateral amygdala. Eur. J. Neurosci. *39*, 1810–1823.

McCormick, D.A., and Contreras, D. (2001). On the cellular and network bases of epileptic seizures. Annu. Rev. Physiol. *63*, 815–846.

McDonald, A.J. (1987). Organization of amygdaloid projections to the mediodorsal thalamus and prefrontal cortex: a fluorescence retrograde transport study in the rat. J. Comp. Neurol. *262*, 46–58.

McDonald, A.J., and Betette, R.L. (2001). Parvalbumin-containing neurons in the rat basolateral amygdala: morphology and co-localization of Calbindin-D28k. Neuroscience *102*, 413–425.

McIntyre, D.C., and Gilby, K.L. (2008). Mapping seizure pathways in the temporal lobe. Epilepsia *49*, 23–30.

Monto, S., Vanhatalo, S., Holmes, M.D., and Palva, J.M. (2007). Epileptogenic neocortical networks are revealed by abnormal temporal dynamics in seizure-free subdural EEG. Cereb. Cortex *17*, 1386–1393.

Motaghi, S., Niknazar, M., Sayyah, M., Babapour, V., Vosoughi Vahdat, B., and Shamsollahi, M.B. (2012). Alterations of the electroencephalogram sub-bands amplitude during focal seizures in the pilocarpine model of epilepsy. Physiol. Pharmacol. *16*, 11–20.

Muller, J.F., Mascagni, F., and McDonald, A.J. (2005). Coupled networks of parvalbumin-immunoreactive interneurons in the rat basolateral amygdala. J. Neurosci. *25*, 7366–7376.

Muller, J.F., Mascagni, F., and McDonald, A.J. (2006). Pyramidal cells of the rat basolateral amygdala: synaptology and innervation by parvalbumin-immunoreactive interneurons. J. Comp. Neurol. *494*, 635–650.

Musto, A.E., Samii, M.S., and Hayes, J.F. (2009). Different phases of afterdischarge during rapid kindling procedure in mice. Epilepsy Res. *85*, 199–205.

Ohshiro, H., Kubota, S., and Murakoshi, T. (2011). Dopaminergic modulation of oscillatory network inhibition in the rat basolateral amygdala depends on initial activity state. Neuropharmacology *61*, 857–866.

Paré, D., Royer, S., Smith, Y., and Lang, E.J. (2003). Contextual inhibitory gating of impulse traffic in the intra-amygdaloid network. Ann. N Y Acad. Sci. *985*, 78–91.

Penfield, W., and Jasper, H. (1954). Epilepsy and the functional anatomy of the human brain. Neurology *4*, 483.

Pinault, D., Vergnes, M., and Marescaux, C. (2001). Medium-voltage 5–9-Hz oscillations give rise to spike-and-wave discharges in a genetic model of absence epilepsy: in vivo dual extracellular recording of thalamic relay and reticular neurons. Neuroscience *105*, 181–201.

Rainnie, D.G. (1999). Serotonergic modulation of neurotransmission in the rat basolateral amygdala. J. Neurophysiol. *82*, 69–85.

Remy, S., and Spruston, N. (2007). Dendritic spikes induce single-burst long-term potentiation. Proc. Natl. Acad. Sci. U S A *104*, 17192–17197.

Schnitzler, A., and Gross, J. (2005). Normal and pathological oscillatory communication in the brain. Nat. Rev. Neurosci. *6*, 285–296.

Siniscalchi, A., Calabresi, P., and Mercuri, N.B. (1997). Epileptiform discharge induced by 4-aminopyridine in magnesium-free medium in neocortical neurons: physiological and pharmacological characterization. Neuroscience *81*, 189–197.

Smith, Y., and Paré, D. (1994). Intra-amygdaloid projections of the lateral nucleus in the cat: PHA-L anterograde labeling combined with postembedding GABA and glutamate immunocytochemistry. J. Comp. Neurol. *342*, 232–248.

Spampanato, J., Polepalli, J., and Sah, P. (2011). Interneurons in the basolateral amygdala. Neuropharmacology *60*, 765–773.

Stafstrom, C.E. (1998). Back to basics: the pathophysiology of epileptic seizures: a primer for pediatricians. Pediatr. Rev. *19*, 342–351.

Steriade, M., and Amzica, F. (2003). Sleep oscillations developing into seizures in corticothalamic systems. Epilepsia *44*, 9–20.

Thomas, M.J., Watabe, A.M., Moody, T.D., Makhinson, M., and O'Dell, T.J. (1998). Postsynaptic complex spike bursting enables the induction of LTP by theta frequency synaptic stimulation. J. Neurosci. *18*, 7118–7126.

Tsuchiya, K., and Kogure, S. (2011). Fast Fourier transformation analysis of kindling-induced afterdischarge in the rabbit hippocampus. Epilepsy Res. *95*, 144–151.

Woodruff, A.R., and Sah, P. (2007a). Networks of parvalbumin-positive interneurons in the basolateral amygdala. J. Neurosci. *27*, 553–563.

Woodruff, A.R., and Sah, P. (2007b). Inhibition and synchronization of basal amygdala principal neuron spiking by parvalbumin-positive interneurons. J. Neurophysiol. *98*, 2956–2961.

Yaari, Y., and Beck, H. (2002). Epileptic neurons" in temporal lobe epilepsy. Brain Pathol. *12*, 234–239.

Yang, Y.-C., Wang, G.-H., Chuang, A.-Y., and Hsueh, S.-W. (2020). Perampanel reduces paroxysmal depolarizing shift and inhibitory synaptic input in excitatory neurons to inhibit epileptic network oscillations. Br. J. Pharmacol. https://doi.org/10.1111/bph.15253.

iScience, Volume *23*

Supplemental Information

Delta-Frequency Augmentation and Synchronization in Seizure Discharges and Telencephalic Transmission

Ping Chou, Guan-Hsun Wang, Shu-Wei Hsueh, Ya-Chin Yang, and Chung-Chin Kuo

Transparent Methods

Animals

All experiments including the care and use of animals were conducted in strict compliance with the recommendations in the Guide for the Care and Use of Laboratory Animals of the National Institutes of Health, USA, and the protocols approved by the Institutional Animal Care and Use Committee of National Taiwan University College of Medicine (Approval Number: 20130443 and 20160391), and that of Chang Gung University (Approval Number: CGU106-081, CGU106-206, CGU107-277, and CGU108-027), Taiwan. All animals were maintained in a vivarium with controlled 12-hour dark/light cycle, and ad libitum access to food and water. Wistar rats and wild-type C57BL/6 mice were purchased from BioLASCO Taiwan Co., Ltd., Taiwan. Thy1-ChR2-eYFP (line 18, #007612) transgenic mice, which express Channelrhodopsin-2 at glutamatergic pyramidal neurons within the basolateral amygdala (Jasnow *et al.*, 2013) were purchased from Jackson Laboratory.

Implantation of electrodes and optic fibers

During stereotaxic surgery, male Wistar rats (6-8 weeks, 250-300 g) were anesthetized by intraperitoneal infusion of 1 ml/kg of normal saline mixture solution containing 50 mg/ml Zoletil 50 (Virbac, France) and 10 mg/ml Xylazine (Sigma Aldrich, USA), and then mounted on a stereotaxic frame (Narishige, Japan). Each rat was implanted with bipolar insulated tungsten electrodes (0.002 inch in diameter, <0.5 mm apart, California Fine Wire Company, USA) into desired brain regions bilaterally following the Paxinos and Watson Brain Atlas for electrophysiology recordings. The kindling stimulation site, however, was always in the left basolateral amygdala (BLA in rats, posterior 3 mm, lateral 5 mm, and deep 8.8 mm relative to bregma), where an

additional pair of electrodes was implanted for stimulation. Two stainless steel screws were wound with silver wires (A-M System, USA) and tighten on the skull above cerebellum as well as on the nasal bone as reference and ground electrodes, respectively. Finally, the electrodes were welded on connectors (Omnetics Connector Corporation) and the scalp wound was covered with dental cement. Following similar procedures, optical fibers (200 μm, 0.37 NA, Newdoon Inc., China) glued with electrodes were implanted into the brain (BLA in mice, posterior 1.5 mm, lateral 3 mm, and deep 4.8 mm relative to bregma) of male Thy1-ChR2-eYFP transgenic mice (6-8 weeks, 20-30 g) for optogenetic stimulation. After surgery, animals were allowed to rest for 1~2 weeks and orally administered with ibuprofen (Sigma Aldrich, USA) in drinking water for 3 days before experiments. After recording, animals were sacrificed with intraperitoneal injection of overdose Zoletil 50. A 5-mA constant current was then passed via the electrodes for 20 sec to cause electrolytic lesions that mark the position of the electrodes. Animals were then perfused with 0.9 % normal saline and 4 % formaldehyde via the ascending aorta. The brain was removed and stored at 4 ˚C in 4 % formaldehyde at least overnight for postfixation, and then stored in 25 % sucrose solution for at least 3 days for cryoprotection. Afterwards the brains were sectioned by a cryotome (CM1950, Leica, Germany) at 30 μm thickness, and stained with cresyl violet acetate (Nissl staining, Sigma Aldrich, USA) to verify the positions of the electrodes. Only the data from the rats with verified correct location of all electrodes are used for further analysis.

In-vivo kindling procedures

At first, a session of 50 Hz biphasic square pulses (1 ms each phase, ±50 μA in amplitude, 10 sec per session) with a stimulus generator (STG4002, Multichannel

Systems, USA) was applied to the left BLA. If there are no afterdischarges (i.e. epileptiform discharges lasting for at least 5 sec) induced after the stimulation session, the procedures were repeated with a current amplitude increment of ±10 μA every 2 min to a maximum of ±300 μA. The current amplitude inducing the first appearance of afterdischarges is defined as the afterdischarges threshold (ADT). Those rats which did not have an ADT ≤ ±300 μA (~2%, 4 out of 24 rats) were not used for further experiments. We then applied sessions of 50 Hz biphasic square pulses (1 ms each phase, 10 sec per session) at ADT (mean ADT = 130 ± 27 μA for 20 rats) for rapid kindling stimulation. The stimulation sessions were repeated every 20 min, 10 times a day for up to 4 days (Morales *et al.*, 2014), and the 20-min period right before the first stimulation in each day was taken as baseline. Behavioral seizure scores were evaluated in every session according to modified Racine's stages (Racine, 1972): stage 0) normal behavior; stage 0.5) epileptiform discharges (afterdischarges), absence-like, freezing behavior; stage 1) facial clonus and mouth clonus; stage 2) head nodding; stage 3) unilateral forelimb clonus; stage 4) bilateral forelimb clonus with rearing; stage 5) rearing and falling; stage 6) wild running and jumping. When an animal progressed into stage-5 or higher seizures for 3 sessions, it was considered as successfully kindled and the kindling protocols were concluded. As a working definition, we also take seizures without vivid convulsions (Racine stages 0.5-2) as low-stage, and those with vivid convulsion or associated violent behaviors (Racine stage 3 and above) as high-stage. All of the 20 included rats (rats that had an ADT ≤ ±300 μA) were successfully kindled. But only the data from 7 rats, which have verified correct positions for all electrodes, were used for further analysis.

In-vivo photostimulation

The blue light for optogenetic stimulation was generated by a 473 nm diode-pumped solid-state (DPSS) laser (Newdoon Inc., China). The stimulation parameters for optical stimulations were controlled by a touch panel and verified with sample recordings. A 50 Hz (1 ms/pulse) light stimulation for 10 sec was applied via an optic fiber to the left BLA to mimic electrical kindling stimulation. The light power was typically changed between 2 to 50 mW (measured at the optic fiber tip) with a step increment as small as 2 mW for ADT measurement. All of the 9 mice show an ADT ≤ 50 mW. We then applied sessions of 50 Hz biphasic square light pulses (1 ms each phase, 10 sec per session) at ADT (mean ADT = 5.6 ± 0.3 mW for 9 mice) for optokindling stimulation. All of the 9 included mice (mice that had an ADT ≤ 50 mW) were successfully kindled. But only the data from 2 mice, which have verified correct positions for all electrodes, were used for further analysis.

In-vivo electrophysiological recording

We recorded in-vivo electrophysiological signals which were band-passed from 0.1 to 3000 Hz with a 40 dB/decade cut-off rate filter and a 60 Hz notch amplified with 1400 gain through an analog amplifier (Model 3600, A-M System, USA), and then digitized with a sampling rate of 25 kHz (DataWave Technologies, USA). To separated local field potentials (LFPs) and multi-unit spikes (MUs), signals were passed through a Butterworth 2^{nd} order infinite impulse response (IIR) filter with 6 dB/oct roll-off to get LFPs (100 Hz low-pass) and MUs (300 Hz high-pass) simultaneously during, or through a finite impulse response (FIR) filter after, the recordings. A 3-axis accelerometer (Analog Devices, USA) was anchored to the headstage (Plexon, USA), measured the acceleration of gravity in tilt-sensing as a motion sensor. The mechanical signals of acceleration of gravity were then converted

to voltage signal and input into amplifier with the same filter and amplification setting.

Signal analysis

LFPs signals were down-sampled to 500 Hz, and characterized in the frequency domain by power spectrum density (PSD) function in Welch's method with Hamming window (with a window length of 1024 points and half of the data overlapped, giving the resolution of 0.488 Hz in each signals; pCLAMP 10, MDS Analytical Technologies, USA). For time-frequency analysis, the first 10-sec segment was taken for analysis and then shifted by 1 sec for the next 10-sec segment until the completion of the full-length signal. Coherence analysis between each two signals was processed under function *mscohere* in Matlab (Mathworks, Natick, USA), defined by squared cross-spectrum between the two signals, and divided by the auto-spectrum of each signal. The value of coherence is between 0 to 1, where 1 indicates that one signal can be linearly transformed into the other one in the frequency domain, and 0 means completely lack of linear relationship. For phase analysis, we calculated instantaneous phase of FIR filter with 21^{st} order Hamming window filtered delta (1-5 Hz) band of LFPs via Hilbert transform (Neuroexplorer, Nex Technologies, USA). If two signals were synchronized, then they have linear correlations in statistics (r = 1 for positive correlation and = -1 for negative correlation). The coefficient of determination (R^2) denotes the square of r, which ranges from 0 to 1 and indicates how well the real values of one signal could fit with the other one with a linear prediction.

To evaluate the synchrony between the MU activities in bilateral BLAs, we took the interspike distance ("SPIKE-distance") in the time axis as the key estimator (Kreuz *et al.*, 2013). The analysis is done by a graphical user interface in Matlab, SPIKY, which

is provided online (Kreuz *et al.*, 2015). SPIKE-distance is derived from the distance between two neighbor spikes in the first train and the closest one in the second train for each spike, and then applied to calculate the "dissimilarity" score (S), which signals the desynchrony of firing patterns rather than single event synchronization. The value of S is between zero and one, and is addressed to measure the differences of timing between two spike trains instantaneously. Zero indicates that the two spike trains are identical or fully synchronized (i.e. no SPIKE-distance differences between the two spikes trains), and one indicates a fully desynchronized condition. We then denote 1 minus S as "similarity", which serves as a more straightforward indicator of the degree of synchronization between the two spike trains. To sorting the single units, the spikes in MUs were detected under a threshold detection algorithm. Specifically, MUs were calculated for average and standard deviation for negative peaks. Three-sigma rule were then applied to extract spikes (i.e. those >3 SD were detected and taken as spikes) (SciWorks 10.0, DataWave Technologies, USA). The extracted spikes were subsequently calculated under principle component analysis (PCA) algorithm, and generated waveform boundary clusters on a PC1vs. PC2 plane. Any waveform that falls below the upper waveform boundary and above the lower waveform boundary will be considered as part of the cluster. The criteria of waveform boundary clustering are as follows: waveform deviation≦3 SD, inter-cluster deviation ≦3 SD, and mean spike number per cluster≧3. To display the LFPs-SUs coupling during afterdischarges, we set the timestamp of each single unit spike as the zero time points, and the oscillating waves in LFP recordings in the flanking 1-sec (0.5 sec on each side) period are realigned and then averaged to get spike-triggered average (STA) waveforms (Neuroexplorer, Nex Technologies, USA). We also calculated

probabilities of each sorted single unit firing in a given phase of the delta cycle. For this purpose, the original data obtained with digitization at 25 kHz were band-filtered into the delta band (1-5 Hz) were computed for their instantaneous phase via Hilbert transform, with each zero phase timestamp taken as the start of a periodic fluctuation. We then documented the spike timestamps at the instantaneous phase of each cycle (Neuroexplorer, Nex Technologies, USA), and plotted spike probabilities as vectors in different degrees. Vectors in each epoch were calculated based on their mean magnitude and direction to get the mean resultant vector in the custom Matlab codes. The magnitude of the mean resultant vector is defined as phase-locking value (PLVs), and the direction of the mean vector is given in the figures in degree. Only those units with a spike count $\geqq 5$ in each epoch were addressed by this analysis.

Brain slice preparation

Wild-type C57BL/6 of both sexes (aged p20-28) were decapitated under isoflurane anesthesia to obtain the brain which was placed into ice-cold oxygenated choline-based cutting solution (containing [in mM] 87 NaCl, 37.5 choline chloride, 25 $NaHCO_3$, 25 glucose, 2.5 KCl, 1.25 NaH_2PO_4, 7 $MgCl_2$, and 0.5 $CaCl_2$). Coronal slices containing BLA (Niittykoski *et al.*, 2004; Sosulina *et al.*, 2010) (270 μm in thickness) were cut on a vibratome (VT1200S, Leica, Germany), and oxygenated in the cutting solution for 20 minutes at 30°C and then in saline (containing [in mM] 125 NaCl, 26 $NaHCO_3$, 25 glucose, 2.5 KCl, 1.25 NaH_2PO_4, 1 $MgCl_2$, and 2 $CaCl_2$) for 20 minutes at 30°C before electrophysiological experiments.

Electrophysiological recording and electrical stimulation in brain slices

The slice was then placed in the recording chamber perfused with oxygenated (95%

O_2/5% CO_2) saline by a peristaltic pump (Gilson Medical Electric, USA) at a stable rate approximately ~5 ml/min. A ×4 objective was used to visualize BLA, and individual neurons were seen with a ×60 water immersion objective on an upright microscope (BX51WI, Olympus, Japan) and were recorded in whole-cell current-clamp mode at room temperature with 3-6 MΩ borosilicate pipettes containing K^+-based solution (in mM, 116 $KMeSO_4$, 6 KCl, 2 NaCl, 20 HEPES, 0.5 EGTA, 4 MgATP, 0.3 NaGTP, 10 $NaPO_4$ creatine, and pH 7.25 adjusted with KOH). A micropipette puller (DMZ-Zeitz-Puller, Germany) was used to make the recording electrodes of borosilicate capillaries (1.65-mm outer diameter, 1.28-mm inner diameter, Harvard Apparatus, USA). Kindling-like stimulation (Goddard *et al.*, 1969; Tuunanen *et al.*, 1997) applied in BLA (1-s train of 0.4-ms monophasic rectangular pulse at frequency of 60 Hz at an intensity of 400 μA, World Precision Instruments A356) was performed by using a paired electrode filled with 0.9% NaCl. The stimulating electrode was placed within the BLA tissue and the grounding electrode placed right above but not touching the surface of BLA slice. We always waited for 4 minutes to ensure full recovery (most neurons can fully recover within 2 minutes after stimulation) between each stimulation session. The signals were amplified with a Multiclamp 700B or axopatch 200B amplifier (MDS Analytical Technologies, USA), sampled at 20 kHz, filtered at 5 kHz, and digitized at 10-20 kHz with a Digidata-1440 analog/digital interface along with pCLAMP software (MDS Analytical Technologies, USA). Usually a current-clamp recording with good quality would last at least 60 min. In pair-recordings, the two neurons are always no more than 300 μm apart.

Identification of BLA pyramidal neurons and interneurons

Neurons in BLA can be separated into two groups, namely pyramidal neurons, and

non-pyramidal or interneurons (Sah *et al.*, 2003). After membrane breakthrough, a depolarizing step current of sufficient magnitude (Mahanty and Sah, 1998) is injected at membrane potential of -60 mV to elicit cellular discharges. Interneurons have smaller diameter and little or no spike frequency adaptation whereas pyramidal neurons possess longer diameter and exhibit prominent spike frequency adaptation in response to current injection (Washburn and Moises, 1992; Rainnie *et al.*, 1993; Mahanty and Sah, 1998; Sah *et al.*, 2003; Spampanato *et al.*, 2011). In this study, we would like to focus on parvalbumin-containing (PV+) INs because they may critically involve in network synchrony in BLA as well as in other structures (Muller et al., 2005; Woodruff and Sah, 2007a; Woodruff and Sah, 2007b; Spampanato et al., 2011; Tremblay et al., 2016). Although some reports have showed that the PV+ INs may have heterogeneous electrophysiological properties, the majority of PV+ INs exhibits no spike frequency adaptation in response to depolarizing step current injection (Rainnie et al., 2006; Woodruff and Sah, 2007a). There are even studies with PV+ INs never showing spike adaptation injected with depolarizing current (Woodruff and Sah, 2007b; Chu et al., 2012). On the other hand, it is generally accepted that PNs show spike adaptation with depolarizing pulses (Sah et al., 2003). We thus limited the sampled INs to those showing no spike frequency adaptation to decrease the likelihood of erroneous inclusion of PNs. We also visualized the morphology of pyramidal neurons and interneurons with immunofluorescent confocal imaging performed on the same acute brain slices used for electrophysiological recordings following protocols developed by McLeod and colleagues (Mcleod et al., 2017). With confocal microscopy (LSM780, Zeiss, Germany), pyramidal neurons and interneurons were identified by immunopositivity of Ca^{2+}/calmodulin-dependent protein kinase II antibody (CaMKII, 1:1000; Biorbyt, UK) and parvalbumin (PV,

1:1000; Synaptic Systems), as well as specific fluorescence in glutamatergic and GABAergic neurons in Thy1-ChR2-eYFP and Gad2-Cre;Ai32 mice , respectively. Ai32 (#024109), Gad2-Cre (#010802) and Thy1-ChR2-eYFP (#007612) transgenic mice were from Jackson Laboratory. In addition, we also used recording electrodes to fill BLA neurons with high concentration (0.4%, for faster labeling) of Lucifer Yellow CH, lithium Salt (Thermo Fisher Scientific, USA) in K^+-based solution, and identified their morphology on a fluorescence microscope. As a working definition, the smaller (longest diameter$\leqq$10 μm) neurons of non-pyramidal morphology that showed little spike frequency adaptation were then identified as interneurons, while larger neurons (longest diameter >12 μm) of pyramidal morphology that exhibit spike frequency adaptation were identified as pyramidal neurons.

In-vitro data analysis

All brain slice recording data were analyzed with pCLAMP 10 (MDS Analytical Technologies, USA), SigmaPlot 12 (Systat Software Inc., USA) and Excel 2013 (Microsoft, USA) software. The definition of burst is modified from Rainnie's group (Rainnie et al., 1993) to count the number of burst discharges in slice recording data. Postsynaptic events having at least one spike on top of rapidly summating high-frequency EPSPs were defined as burst discharges (Rainnie et al., 1993). Only EPSPs and IPSPs with amplitude greater than 3 mV were included in analysis. When two cells were recorded simultaneously, any two postsynaptic events (burst discharges, EPSPs or IPSPs, each from different neurons in a pair-recording) recorded in the two cells, respectively, having a difference in the onset time <50 ms are defined as synchronized events. For the pre-kindling and post-kindling parameters, each analysis was based on the data averaged from a 45-sec continuous stable recording just

before and after the stimuli, respectively. The burst duration and inter-burst interval were measured and analyzed in pCLAMP 10. The sample size denotes the number of neurons.

Statistics

Mann-Whitney U test and Wilcoxon signed-rank test were used for statistical comparison (Prism 6, GraphPad, USA), which were two-sided and the p-values < 0.05 were accepted as significant difference. The software used to analysis are Prism 6.01 (GraphPad, USA) and PASW statistics for windows, version 18.0 (SPSS, USA) for in-vivo and in-vitro data, respectively. All data are shown as means ± SEM.

Supplemental References

Chu, H.Y., Ito, W., Li, J., Morozov, A. (2012). Target-specific suppression of GABA release from parvalbumin interneurons in the basolateral amygdala by dopamine. Journal of Neuroscience, 32(42), 14815-14820.

Goddard G.V., McIntyre D.C., Leech C.K. (1969). A permanent change in brain function resulting from daily electrical stimulation. Exp Neurol 25(3): 295-330.

Kreuz T., Chicharro D., Houghton C., Andrzejak R.G., Mormann F. (2013). Monitoring spike train synchrony. J Neurophysiol 109(5): 1457–72.

Kreuz T., Mulansky M., Bozanic N. (2015). SPIKY: a graphical user interface for monitoring spike train synchrony. J Neurophysiol 113(9): 3432–45.

Mahanty N.K., Sah P.J.N. (1998). Calcium-permeable AMPA receptors mediate long-term potentiation in interneurons in the amygdala. Nature 394(6694): 683–7.

McLeod F., Marzo A., Podpolny M., Galli S., Salinas P. (2017). Evaluation of Synapse Density in Hippocampal Rodent Brain Slices. Jove-J. Vis. Exp. 128, e56153.

Morales, J.C., Alvarez-Ferradas C., Roncagliolo M., Fuenzalida M., Wellmann M., Nualart F.J., Bonansco C. (2014). A new rapid kindling variant for induction

of cortical epileptogenesis in freely moving rats. Front Cell Neurosci 8: 200.

Muller J.F., Mascagni F., McDonald A.J. (2005). Coupled networks of parvalbumin-immunoreactive interneurons in the rat basolateral amygdala. J. Neurosci. 25, 7366-7376.

Jasnow A.M., Ehrlich D.E., Choi D.C., Dabrowska J., Bowers M.E., McCullough K.M., Rainnie D.G., Ressler K.J. (2013). Thy1-Expressing Neurons in the Basolateral Amygdala May Mediate Fear Inhibition. J Neurosci 33(25), 10396-10404.

Racine R.J. (1972). Modification of seizure activity by electrical stimulation: II. Motor seizure. Electroencephal Clin Neurophysiol 32(3): 281–94.

Rainnie D.G., Asprodini E.K., Shinnick-Gallagher P. (1993). Intracellular recordings from morphologically identified neurons of the basolateral amygdala. J Neurophysiol 69(4): 1350–62.

Rainnie D.G., Mania I., Mascagni F., McDonald A.J. (2006). Physiological and morphological characterization of parvalbumin-containing interneurons of the rat basolateral amygdala. Journal of Comparative Neurology, 498(1), 142-161.

Sah P., Faber E.S., Lopez De Armentia M., Power J. (2003). The amygdaloid complex: anatomy and physiology. Physiol Rev 83(3): 803–34.

Spampanato J., Polepalli J., Sah P. (2011). Interneurons in the basolateral amygdala.

Neuropharmacology 60(5): 765–73.

Tremblay R., Lee S., Rudy B. (2016). GABAergic interneurons in the neocortex: from cellular properties to circuits. Neuron, 91(2), 260-292.

Tuunanen J., Halonen T., Pitkänen A. Decrease in somatostatin-immunoreactive neurons in the rat amygdaloid complex in a kindling model of temporal lobe epilepsy (1997). Epilepsy Res 26(2): 315–27.

Washburn M.S., Moises H.C. (1992). Electrophysiological and morphological properties of rat basolateral amygdaloid neurons in vitro. J Neurosci 12(10): 4066–79.

Woodruff A.R., Sah P. (2007a). Networks of parvalbumin-positive interneurons in the basolateral amygdala. J Neurosci 27(3): 553–563.

Woodruff A.R., Sah P. (2007b). Inhibition and synchronization of basal amygdala principal neuron spiking by parvalbumin-positive interneurons. J Neurophysiol 98(5): 2956–61.